## General Disclaimer

## One or more of the Following Statements may affect this Document

- This document has been reproduced from the best copy furnished by the organizational source. It is being released in the interest of making available as much information as possible.

- This document may contain data, which exceeds the sheet parameters. It was furnished in this condition by the organizational source and is the best copy available.

- This document may contain tone-on-tone or color graphs, charts and/or pictures, which have been reproduced in black and white.

- This document is paginated as submitted by the original source.

- Portions of this document are not fully legible due to the historical nature of some of the material. However, it is the best reproduction available from the original submission.

NASA Technical Memorandum 82890



# QCSEE Under-the-Wing Engine-Wing-Flap Aerodynamic Profile Characteristics


Harry E. Bloomer and Nicholas E. Samanich
*Lewis Research Center*
*Cleveland, Ohio*

September 1982

NASA

# QSCEE UNDER-THE-WING ENGINE-WING-FLAP AERODYNAMIC PROFILE CHARACTERISTICS

Harry E. Bloomer and Nicholas E. Samanich

National Aeronautics and Space Administration
Lewis Research Center
Cleveland, Ohio

## SUMMARY

As part of a broad-based NASA program to provide a technology base for future propulsion requirements for powered-lift aircraft, the Quiet, Clean, Short-Haul, Experimental Engine (QCSEE) program was begun by the Lewis Research Center in 1974. The initial buildup of the under-the-wing (UTW) engine was tested by the contractor at his test site. The UTW engine was delivered to Lewis in 1978 for further testing with wing and flap segments simulating an installation on a shorthaul transport aircraft. The engine was also tested alone as an aid in identifying the various noise sources and their levels. As part of these tests the aerodynamic profiles at the exhaust nozzle and on the surfaces and in the wake of the wing-flap system were measured. This report documents, in plots and in tabular form, the significant results from those tests. The results are presented as tabulations of aerodynamic data for all of the test points and as profiles of pressure, temperature, velocity, and normalized velocity and pressure for selected conditions. One of the main conclusions was that the measured flap surface temperatures were surprisingly low for both approach and takeoff flap settings.

## INTRODUCTION

Two experimental engines, an over the wing (OTW) and an under the wing (UTW), were designed and built under the Quiet, Clean, Short-Haul, Experimental Engine (QCSEE) program (refs. 1 and 2). The UTW design is reported in reference 3. The initial buildup of the UTW engine was tested by the contractor at his test site. Initial UTW acoustic test results are reported in reference 4. The UTW engine was inspected, refurbished, and delivered to Lewis in 1978 for further testing. Other results of QCSEE testing at Lewis are presented in references 5 to 7.

The engine incorporated many low-noise design features, including a hybrid inlet, wide rotor-stator spacing, frame treatment and treated vanes, stacked treatment in the core to attenuate both turbine noise and low-frequency core noise, and removable fan exhaust wall panels and splitter. Details of the acoustic design are contained in references 8 and 9.

The UTW engine had a variable-geometry fan exhaust nozzle and a variable-pitch fan to provide quick-response reverse thrust capability. An automatic digital control (ref. 10) enabled optimal engine operation under all steady-state conditions as well as during forward and reverse thrust transient operation.

The engine was tested at the Lewis Engine Noise Test Facility with wing and flap segments simulating an installation on a short-haul transport aircraft. The engine was also tested alone as an aid in identifying the various noise sources and their levels. Results of 14 acoustic test configurations are reported in reference 11. The fan blade angle was varied from $+5.2^\circ$ to $-7.6^\circ$ and the exhaust nozzle area was varied from 1.52 to 1.87 $m^2$ (2350 to 2900 $in^2$) in order to

simulate both approach and takeoff power conditions. The jet-flap noise measured in the acoustic tests was dependent on the flow field around the wing-flap system. Therefore, as part of these tests, the aerodynamic profiles at the exhaust nozzle and on the surfaces and in the wake of the wing-flap system were measured. This report documents, in plots and in tabular form, the significant results from those tests. The results are presented as tabulations of aerodynamic data for all of the test points and as profiles of pressure, temperature, velocity, and normalized velocity, pressure, and temperature for selected conditions.

## APPARATUS AND PROCEDURE

### UTW Experimental Propulsion System

The UTW experimental propulsion system, shown in figure 1, featured a composite-structure, high-Mach-number (accelerating) inlet; a gear-driven, variable-pitch fan with composite fan blades; a composite fan frame; an acoustically treated fan duct with an acoustic splitter ring; a variable-geometry fan exhaust nozzle; an advanced (F-101) core and low-pressure turbine; an acoustically treated core exhaust nozzle; top-mounted engine accessories; and a digital electronic control system combined with a hydromechanical fuel control.

The fundamental engine design criteria were influenced by the fan engine cycle required to meet total system noise objectives, which were dictated by jet-flap noise constraints. The acoustic design features of the engine are presented in figure 2. The fan was a low-pressure-ratio (1.27), low-tip-speed (289.6 m/sec, 950 ft/sec) configuration sized to provide 405.5 kg/sec (894 lb/sec) of corrected airflow. The fan contained 18 composite, variable-pitch fan blades with flight-weight disks and blade supporting system. The fan was driven by the F-101 low-pressure turbine through a main reduction gear. The reduction gear was a six-star epicyclic configuration with a gear ratio pf 2.465 and a takeoff power rating of 9806 kW (13 145 hp).

The fan was capable of blade pitch change from forward to reverse thrust through either flat pitch or stall pitch. Two variable-pitch fan actuation systems were developed for the UTW experimental engine: a cam/harmonic drive system developed by the Hamilton Standard Division of United Technologies Corporation under subcontract to the General Electric Company, and a ball spline actuation system developed by General Electric. The rotary motion power required to drive both systems was provided by hydraulic motors. Both systems were designed to move the blades from their forward thrust position to reverse in less than 1 sec.

The fan frame was a flight-weight composite structure containing integral acoustic treatment, outer casing blade containment, and fan tip treatment. The 33 integral outlet guide vanes also acted as structural supports. The outer casing of the frame provided both inner and outer nacelle flow paths. The core inlet flow path and the mounts for the forward bearings, gears, radial drive, etc., were also integrally provided.

The nacelle components included a lightweight composite hybrid inlet that provided acoustic suppression at takeoff power by means of a high throat Mach number (0.79) and structurally integrated acoustic treatment. The composite fan duct, acoustic splitter, and core cowl were hinged from the pylon to provide access for engine maintenance. The core exhaust nozzle and nozzle plug were acoustically treated to reduce aft-radiated noise. The fan exhaust nozzle was a variable-area,

four-flap design capable of area change from takeoff to cruise, as well as opening to a flared position to form an inlet in the reverse thrust mode. The nozzle flaps were hydraulically actuated.

Engine fuel flow, blade pitch angle, and exhaust nozzle area were controlled by a digital electronic control. Major engine accessories were mounted on a boilerplate gearbox on top of the fan frame.

The UTW experimental propulsion system was designed to provide 81 400 N (18 300 lb) of uninstalled thrust and 77 400 N (17 400 lb) of installed thrust at takeoff on a 305.6 K (90° F) day.

Table I lists the design parameters of the engine. Table II lists "as tested" values of pertinent parameters.

## Engine and Wing Configurations

The wing-flap segment used in the UTW program was a modified two-flap NASA supercritical airfoil design recommended by NASA Langley Research Center for short-haul aircraft and described in reference 12. Coordinates for the wing, vane, and flap are given in tables III, IV, and V, respectively. The location of the engine relative to the wing-flap system was based on Langley data that indicated good powered-lift performance. No consideration was given, however, to acoustic optimization. Wing-flap configurations included four different settings of the flap trailing-edge angle $\psi_f$, as shown in figure 3. However, aerodynamic profiles for these tests were obtained only for a takeoff setting of $\psi_f = 20°$ and an approach setting of $\psi_f = 60°$ (configurations B and D). Details of the vane and flap in the cruise position are shown in figure 4(a) and in the approach and takeoff positions in figure 4(b). The flap angles were measured from the main wing segment chord centerline, which was pitched up 5° with respect to the engine's centerline. Dimensions of the engine and the wing and flap cross sections are also shown in figure 3. The separation distance ratio $X/D$ was about 5 at takeoff and 4 at approach, where $X$ is the distance from the fan exhaust exit plane to the wing flaps measured along the engine centerline, and $D$ is the engine open-fan exhaust nozzle diameter (1.9 m, 6.2 ft). The engine centerline was 4.57 (15 ft) above ground level. The span of the vertically mounted wing-flap segment was 7.31 m (24 ft), with the upper edge 7.92 m (26 ft) above ground level.

## Facility

The test program was performed at the Engine Noise Test Facility located at Lewis. The facility is shown in figure 5. More details of the facility are given in reference 7.

## Aerodynamic Instrumentation for UTW Wing and Flap

Shown in figure 6 are scaled layouts of the engine-wing-flap system tested. The flow-measuring instrumentation included a traversing probe to measure engine exhaust velocity at the core nozzle exit plane (station 1), fixed-boundary-layer total pressure rakes in the wing-vane gap (station 1A) and just ahead of the trailing edge of the flap (station 2), and a "super rake" immediately behind the trailing edge of the flap (station 3).

The probe that traversed the nozzle exit plane (station 1) contained single total pressure, total temperature, and static pressure instruments (fig. 7) and was operated by an electrically driven, screw type of linear actuator over a distance of about 100 cm (39 in.).

The rakes used between the trailing edge of the wing and the vane (station 1A) had total pressure tubes 2.5 cm (1 in.) apart (fig. 8). As can be seen in the figure, the rake for the approach flap configuration spanned a flow passage 14.9 cm (5.87 in.) wide, and the rake for the takeoff flap configuration spanned a passage 17.9 cm (7.04 in.) wide.

The boundary layer rake used at station 2, 0.6 cm (0.24 in.) ahead of the trailing edge of the flap, is detailed in figure 9. Six total pressure tubes over both top and bottom surfaces were provided.

The super rake was a large rake containing total pressure, static pressure, and total temperature sensing elements. It was mounted horizontally on a forklift truck that was situated behind the trailing edge of the flap (figs. 5(b) and 6). A schematic drawing of the super rake is shown in figure 10(a). A closeup view of the rake, as it was mounted in another investigation, is presented in figure 10(b).

The spanwise locations of the surface temperature and static pressure measurements on the vane and flap are detailed in figure 11(a). Locations of the thermocouples and pressure probes at each spanwise station are shown in figure 11(b).

## Methods of Recording and Computing Results

A small on-site computer was used to sequence the data acquisition, and a large central data collector was employed to store it. After a "steady state" engine condition was set, the recorders were energized and the exhaust nozzle traversing probe was set in motion from a "home" position outside the fan flow to the inner edge of the core flow, where it was stopped by a limit switch approximately 3 cm (1.2 in.) from the core nozzle inner core surface. During that traverse (approx 50 sec), 100 scans of eight channels of data from the traversing probes and one channel of fan speed were recorded. In the next 30 sec, 600 channels of pressures, temperatures, and other parameters were recorded on the central data collector. A simple computer program converted these raw data into engineering units. After data editing, a complex computer program made up of parts of three existing programs calculated and plotted final results. Some of the equations used are presented in appendix A, and all of the symbols are defined in appendix B.

## Experimental Methods

Before each test series, the super rake and the small trailing-edge boundary layer rake were positioned at one of the predesignated spanwise locations. Then the engine was started and data were obtained at fan speeds of 81 to 95 percent of rated corrected speed. Fan blade angle was varied from $+5.2^\circ$ to $-7.6^\circ$, and the exhaust nozzle area was varied from 1.49 to 1.87 $m^2$ (2310 to 2900 $in^2$) in order to simulate both approach and takeoff power conditions as shown in the following table:

| Power condition | Fan speed, percent of rated corrected | Exhaust nozzle area | | Fan blade angle, deg |
|---|---|---|---|---|
| | | $m^2$ | $in^2$ | |
| Approach | 95 | 1.87 | 2900 | +5.2 |
| Takeoff | [a]95 | 1.49 | 2310 | -7.6 |

[a]Takeoff rated speed was limited by turbine inlet temperature.

The engine was then shut down, the positions of the super rake and the boundary layer rake were changed, and the data-taking process was repeated. Two spanwise positions were run for the approach wing-flap configuration. Four spanwise locations were run for the takeoff wing-flap configuration because the higher exhaust velocities and temperatures for that configuration were deemed to be more critical from a wing-flap structural standpoint.

Traversing probe data were obtained for only one set of conditions since it was felt that the flap configuration would have negligible effect on the exhaust profile in the exit plane (station 1).

## Presentation of Data

The total number of data points taken are listed in table VI along with the other pertinent parameters of the configurations and the engine settings. The traversing probe temperature sensor was inoperative for the first 17 runs but was operative for a full set of engine conditions from run 18 to run 23, inclusive. After these data were obtained, the probe was removed for the remainder of the tests. Note that run 8 was at takeoff power setting with the wing-flap in the approach position to simulate an aborted landing, which would subject the wingflap to the highest thermal and pressure loads. Also note that runs 22, 28, and 38 were at takeoff power settings, which were set by opening up the exhaust nozzle just enough so that 95 percent of rated fan speed could be set at the rated turbine inlet temperature. The other takeoff power runs (8, 14, 21, 24, 30, and 37) were limited by turbine inlet temperature to 94 percent of rated fan speed at an exhaust nozzle area of 1.49 $m^2$ (2310 $in^2$).

The results are discussed in terms of the effect of engine setting condition (i.e., percent of rated fan speed and exhaust nozzle area). The velocity profiles are presented for all of the instrumentation stations. The combined normalized velocity profiles are then presented and compared with model data. Next wake temperatures and surface temperatures and pressures are discussed. Finally, the boundary layer at the flap trailing edge is examined in detail and compared with theory.

## Station 1 - Nozzle Exit Profiles

The velocity profiles in the nozzle exit plane (station 1) are presented in figure 12 for a range of corrected fan speeds from 81 to 94 percent of rated speed

at an exhaust nozzle area of 1.49 $m^2$ (2310 $in^2$). Increasing the fan speed from 81 to 94 percent of rated speed increased the core stream peak velocity from 206 to 261 m/sec (676 to 856 ft/sec) and the fan stream peak velocity from 190 to 214 m/sec (623 to 702 ft/sec). A velocity minimum occurred between the core and fan streams at about 21 cm (8.3 in.), and the velocity of the fan stream dropped off sharply 70 cm (27.6 in.) from the centerline. The core nozzle velocity profile was typical in that the highest velocity occurred toward the outer part of the annulus as a result of the turbine outlet profile and the tendency of the flow to separate from the nozzle centerbody.

Shown in figure 13 is the effect of exhaust nozzle area and fan blade setting on the velocity profile at station 1. When the exhaust nozzle was opened to its maximum area, the fan blades had to be off-loaded to maintain 95 percent of rated fan speed, and the result was a reduction in the peak fan velocity from 215 to 174 m/sec (705 to 570 ft/sec) and in the peak core velocity from 262 to 209 m/sec (860 to 686 ft/sec). In addition to changes in peak velocity, the indicated velocity on the outer fringes of the fan stream was higher for both traverses than for those in figure 12. The average velocity from distances of 90 to 105 cm (35.4 to 41.3 in.) was about 15 m/sec (49 ft/sec) for all four runs in figure 12 with the nozzle closed (1.49-$m^2$ area). Keep in mind that this survey was taken at a 180° vertical position on the bottom of the nozzle directly downstream of one of the four "notches" between nozzle flaps (fig. 5(b)). When the fan exhaust area was 1.54 $m^2$ (2390 $m^2$), there was a small notch between the flaps, and the velocity 100 cm (39.4 in.) from the engine centerline was about 38 m/sec (125 ft/sec) at takeoff power. Opening the nozzle further to 1.87 $m^2$ enlarged the notch between the flaps, but the lower fan pressure ratio at approach power resulted in a velocity at 100 cm (39.4 in.) of about 22 m/sec (72 ft/sec). Another notch between the nozzle flaps at 90° clockwise position directed the flow at the wing-flap surface. It was felt that most of this "bulge" in flow would "wash out" in the turbulent mixing process within a distance of a few nozzle diameters downstream of station 1.

## Station 1A - Wing-Vane Gap Profiles

The effect of fan speed on the velocity profiles at station 1A between the wing trailing edge and the top surface of the vane for the approach flap setting is presented in figure 14. As is rather apparent, there is no effect of fan speed. One curve drawn through the clustered points peaking at about 40 m/sec (131 ft/sec) at a distance of about 12 cm (4.7 in.) from the wing describes the profiles.

Shown in figure 15 is the velocity profile at station 1A for the approach power condition. The fan blade angle had been changed from -7.6° to +5.2° and the exhaust nozzle was opened from 1.49 to 1.87 $m^2$. Also shown for reference is the curve from figure 14. The peak velocity is almost 100 m/sec (328 ft/sec) for the approach condition with the open exhaust nozzle. Although it was not obvious from the profile at station 1 (fig. 13), the open exhaust nozzle resulted in much more flow passing through the gap between the wing and flap than occurred with the nozzle closed.

The station 1A velocity profiles for the takeoff flap setting show about the same insensitivity to fan speed (fig. 16) as was observed for the approach flap setting. One curve drawn through the clustered points with a peak velocity near the vane surface of about 62 m/sec (203 ft/sec) describes the data.

The approach power setting (fig. 17) with the open nozzle (1.87 $m^2$) and the change in fan blade angle from -7.6° to +5.2° again increased the velocity through

the gap. The peak velocity of about 115 m/sec (377 ft/sec) was almost twice that both for the data from figure 16 and for the takeoff power setting with the 1.54-$m^2$ exhaust nozzle area.

## Station 3 - Flap Trailing-Edge Profiles withh Super Rake

The super rake contained its own static pressure probes, which were well designed for minimum error in velocity head. According to reference 13, a flow misalignment of 15° with the axis of the stream tube would result in an error of 6 percent in velocity head. It was felt that the local static pressure near the flap surface would be higher than the ambient static pressure because the local flow compressed on impact with the flap. Also, the bending of the jet streamlines near the flap should have caused the flow to be approximately parallel to the flap angle. On the other hand, at increasing distance from the flap surface, the flap influence on the flow would decrease until at some distance free jet flow would exist. Because of this reasoning, the super rake was positioned at a compromise angle of 105° from the chord line of the flap for both approach and takeoff flap settings (fig. 6) so that any errors in static pressure near or away from the flap would be minimized.

Velocities were calculated by using both measured rake static pressure and barometric ambient static pressure. Results obtained with both methods of calculation are compared in figures 18 and 19 for approach and takeoff flap settings, respectively.

For the approach flap setting at approach power (fig. 18), at a distance from the base of the rake support of 0 to about 60 cm (24 in.), the results from both methods of calculation agreed. From 60 to 82 cm (24 to 32 in.), the rake static calculation yielded a slightly lower velocity, indicating that for the steep angle of the approach flap some of the flow, which was compressed on the bottom surface of the flap, influenced the three stream statics on the rake at 66, 71, and 76 cm (26, 28, and 30 in.). Keep in mind that the rake was located at station 3, which was 4.5 cm downstream of the trailing edge. The velocity calculated by using the rake statics was lower at distances of 82 to 132 cm (32 to 52 in.). Because of the compression referred to earlier, the calculation based on ambient pressure was in error. From a distance of 142 cm (56 in.) to the end of the rake (213.4 cm, 84 in.) the velocity calculated by the rake statics was higher than that calculated by using ambient pressure. The discrepancy between the two methods of calculation is due only to the difference in measured static pressure. The measured rake static pressure was undoubtedly in error because of the extreme flow angularity of the free jet flow. For the takeoff flap (fig. 19) the aforementioned compression effect appeared to influence the rake static pressure at 76 cm (30 in.) and continued to about 170 cm (67 in.). From 170 cm (67 in.) to the end of the rake, the results from both methods of calculation agreed.

After examination of the results from both velocity calculation methods, it was decided that the rake static measurements provided the most accurate velocity in the region of greatest interest near the flap. Therefore the velocity based on rake statics is presented in the remainder of this discussion.

Presented in figure 20 is the effect of fan speed on the velocity survey at the intersection of station 3 and spanwise station A, station 3A, on the engine centerline (fig. 11(a)) for the approach flap setting. Although data were not available for three of the runs at fan speeds of 85, 90, and 94 percent of rated speed at distances to 105 cm (41 in.), the effect of fan speed was small but, generally speaking, the higher the fan speed, the greater the velocity. Note also that the high-velocity region for the 81 percent data is a rather flat plateau

extending from the flap trailing edge to a distance of about 110 cm (43 in.), about 30 cm (12 in.) from the flap surface, with the peak occurring at the flap surface. This indicates that the flow left the flap surface in the form of a wall jet.

Shown in figure 21 is the effect of fan speed on velocity at station 3A for the takeoff flap setting. Again, the effect of fan speed was not large except for the peak that occurred at 127 cm (50 in.) (about 50 cm (20 in.) from the surface) and amounted to an increase in velocity from 167 to 210 m/sec (548 to 689 ft/sec) as the fan speed was increased from 81 to 94 percent of rated speed. Note that the general shape of the profile indicates that the high-velocity core jet apparently did not penetrate through the lower velocity fan jet to the flap surface but was instead turned by the wing-flap system. This contrasts with the results of the approach flap setting at approach power (fig. 18), where the peak velocity occurred near the bottom surface of the flap.

## Combined Normalized Velocity Profiles

Normalized velocity profiles are presented in figure 22 for the approach flap setting at approach power. The velocities have been normalized by dividing by an effective mean (mass average) jet velocity $V_E$, which is defined in the methods of calculation (appendix A). Velocity vector distributions in the plane of the engine and span centerlines (fig. 22(a)) and along the span (fig. 22(b)) are presented. The peak velocity of the core jet at the exhaust exit (station 1) was 1.30 and that of the fan jet was 1.08. The small amount of exhaust passing through the first slot between the wing and the vane had a peak velocity of 0.64. Peak velocity of the deflected exhaust at the flap trailing edge had decayed to 0.87. Spanwise (fig. 22(b)), the peak velocity of station 3B (91 cm (36 in.) from the engine) had diffused to 0.81.

Presented in figure 23 are the combined normalized velocity profiles for the takeoff flap setting at takeoff power. The peak velocity of the core jet was 1.18 and that of the fan jet was 0.96. The peak velocity at station 1A was 0.29 and the peak velocity at station 3A was 0.95. Spanwise, the peak velocity diffused rapidly to peaks of 0.76 at station 3B, 0.40 at station 3C, and 0.23 at station 3D.

## Comparison of Spanwise Velocity Profiles with Model Data

Reference 14 contains model externally blown flap aerodynamic profile data obtained for the QCSEE program. The spanwise velocity profile data for the approach flap have been nondimensionalized and are compared in figure 24 with the full-scale data obtained in this investigation.

The reference investigation employed a single circular convergent nozzle supplied with pressurized air to simulate the engine. The effective throat diameter of the nozzle was 9.3 cm (3.7 in.) and the wing chord was 32 cm (12.6 in.) with the flaps retracted. The spanwise distance $Y$ and the vertical distance above or below the flap $Z$ were nondimensionalized by dividing by the wing chord $C$. The $Z/C$ value for the model data was 0.03125, which translates to 18.65 cm (7.3 in.) for the full-scale data. Since only two spanwise positions of the super rake were obtained for the approach flap, the shape of the curve is indeterminate, but the general level of the curve appears to correspond to levels obtained with the model data.

Presented in figure 25 is another spanwise velocity profile comparison from reference 14 model data with the full-scale data for the takeoff flap setting at takeoff power. These data have also been nondimensionalized in the same manner as previously discussed. The Z/C value of 0.0834 translates to 49.8 cm (19.6 in.) for the full-scale data. The generalshapes of the curves are similar. The level of the full-scale data is somewhat higher than the model data at distances from the centerline Y/C to about 0.225. At Y/C greater than 0.225, the full-scale data are lower than the model data. The reason for this variation may be the difference in spreading characteristics between a single convergent nozzle used in the model tests and the coannular fan jet and core jet used in the full-scale tests. Another reason could be that the mass-averaged Mach number for a coannular jet may only be roughly equivalent to the jet Mach number calculated for the model jet. Even so, the comparison between the two sets of data was good.

## Combined Temperature Profiles

Exhaust gas temperature profiles are shown at the nozzle exit station and in the wake behind the flap trailing edge, along with wing-flap skin temperatures, in figure 26. Data are presented for the approach power setting and the approach wing-flap configuration. Note that none of the wing-flap skin temperatures are very high even though the 1554° R (1094° F) core jet was directed at the flap surface. The maximum flap skin temperature was 619° R (159° F) on the centerline at the trailing edge. The higher values of the temperature profile, unlike the higher values of the velocity profile of figure 22, were measured at locations shielded from the surface of the flap by the relatively cool fan jet stream. The maximum temperature at station 3A, 774° R (314° F), occurred well away from the surface of the flap. This can also be observed in figure 26(b), where spanwise measured temperature ratioed to maximum gas temperature $T_N$ is presented. Spanwise (fig. 26(b)), the skin temperature dropped to 564° R (104° F) at a distance of 305 cm (120 in.) from the centerline. An ambient temperature is shown in both figures for reference.

Presented in figure 27 are the temperature profiles in the plane of the engine and span centerlines (fig. 27(a)) and spanwise (fig. 27(b)) for the takeoff power setting and the takeoff wing-flap configuration. Again, ambient temperature is shown in both figures for reference. The maximum nozzle gas temperature, 1755° R (1295° F), dropped to 1138° R (678° F) at station 3A. The maximum vane skin temperature was 610° R (150° F) and the maximum flap skin temperature was 586° R (126° F). Spanwise, the skin temperature at the trailing edge of the flap decreased to 555° R (95° F) at a distance of 305 cm (120 in.) from the centerline. The normalized maximum temperature at station 3 $T/T_N$ occurred 50 cm (20 in.) below the flap trailing edge.

## Vane and Flap Bottom-Surface Temperature Contours

Shown in figure 28 are bottom-surface temperature contours for three conditions: approach flap setting at approach power (fig. 28(a)); approach flap setting at takeoff power (fig. 28(b)), to illustrate the most severe conditions during an aborted landing; and takeoff flap setting at takeoff power (fig. 28(c)). All temperatures were normalized by the ambient temperature $T_0$.

At approach power and approach flap setting no skin temperature problem existed, with a maximum temperature of 616° R (156° F) ($T/T_0 = 1.15$) measured at the flap trailing-edge centerline. The absence of a skin temperature problem was

somewhat surprising since a previous program (ref. 15) on STOL aircraft indicated that the engine nozzle should be canted down 9° to avoid impingement of the hot exhaust gases on the flap surface.

For the approach flap setting at takeoff power (fig. 28(b)) contours are similar except that the maximum normalized temperature was higher (1.24 versus 1.15) for takeoff power than for approach power (fig. 28(a)). Even though the aborted landing condition would be a rather transient one, the skin temperatures were not excessively high for standard aircraft wing structures. The maximum measured skin temperature was 668° R (208° F) for takeoff power.

For the takeoff flap setting at takeoff power (fig. 28(c)) the skin temperatures were lower than for either of the two approach conditions. The maximum normalized temperature was only 1.08. The general shapes of the contours are similar to those for the two approach conditions.

## Vane and Flap Bottom-Surface Pressure Contours

Shown in figure 28 are bottom-surface vane and flap static pressure contours. The pressures have been normalized by the ambient pressure $P_0$. For the approach flap setting at approach power, the highest pressure was 1.10 and it occurred about midchord on the flap slightly outboard of the centerline. The engine centerline target was about midchord of the flap (fig. 6(b)). The results presented here are typical of a strong interaction between large-scale turbulence structures and the flap as pointed out in reference 14, where the flow reorganized after impact and left the trailing edge of the flap in the form of a wall jet.

When the power was increased to takeoff at the approach flap setting (fig. 29(b)), the maximum pressure increased to 1.17 and the location of the maximum pressure lobe shifted forward on the flap in comparison with its approach power position (fig. 29(a)). Other than those differences, the contours on the flap were somewhat similar in shape. However, the leading edge of the flap had pressures slightly less than ambient, an indication that the flow stagnation pressure point had moved downward below the first static pressure ports and the flow had reversed itself to flow over the top of the flap from that point.

Changing the wing flap to the takeoff setting at takeoff power (fig. 29(c)) reduced the maximum pressure lobe to 1.06 and moved it downstream. The pressures at the leading edge of the flap were above ambient pressure. There was evidence of some flow separation around the curve on the bottom of the vane near the center of the chord. However, not enough pressure taps were installed to adequately define the pressure contours over the vane surface. Data from reference 16 indicated that separation did occur at this condition.

## Flap Top-Surface Pressure Contours

Presented in figure 30 are the flap top-surface static pressure contours for the same conditions that were presented in figure 29. Even though the number of pressure taps was limited, some representation of the flow can be derived from the pressure contours presented. In figure 30(a), for the approach flap setting at approach power, the high velocity over the leading edge produced a $P/P_0$ of 0.94. Even though an adverse pressure gradient existed on the flap top surface and the pressure ratio rose above 1, flow separation did not occur, as discussed in the following section.

Shown in figure 30(b) is the same approach flap setting at takeoff power. There are no significant differences from the preceding (approach power) figure.

Changing the flap setting to takeoff at takeoff power (fig. 30(c)) did change the contours somewhat. The lowest measured pressure ratio increased from 0.94 for the approach flap setting to 0.98 for the takeoff flap setting.

## Boundary Layer Characteristics at Flap Trailing Edge, Station 2

The effect of engine exhaust jet Mach number on the boundary layer survey at the flap trailing edge, station 2A (figs. 6 and 11), is presented in figure 31. Jet Mach number was based on the effective (core plus fan) velocity and temperature, as shown in appendix A. The boundary layer velocities were calculated by using the ambient static pressure and the average of the nearest two super-rake temperatures on each side of the flap trailing edge. For both flap settings, as the jet Mach number was increased, the main-stream velocity increased, as would be expected. Within the narrow range of jet Mach numbers (0.425 to 0.572) the indicated boundary layer thickness did not change. One questionable aspect of the profile for both flap settings is that the pressure tube nearest the bottom surface indicated a higher velocity than any of the otner tubes. Assuming that the nearest flap-surface static pressure, which was within 15 cm (6 in.) of the boundary layer rake, was more indicative of the true static pressure, the calculated velocity for that one tube can be lowered. For the boundary layer on the top surface of the flap, the assumption can be made that the suction-surface static pressure would be more descriptive of the boundary layer rake environment than the measured ambient pressure. Incorporating these assumptions resulted in the boundary layer profiles shown in figure 32. Both approach flap setting at approach power (fig. 32(a)) and takeoff flap setting at takeoff power (fig. 32(b)) are presented. The velocities shown over the top surface are higher than those shown in figure 31 because the suction-surface pressures were lower than ambient. The boundary layers are typical of those over the top surface of any airfoil for subsonic flow conditions. Calculating a boundary layer thickness by using the method in reference 17 with a Reynolds number based on the chord length of the flap resulted in a thickness of about 3 cm (1.2 in.) for both conditions presented. This calculated value appears to be confirmed by the experimental data. Of more importance, however, (especially in noise calculations) is the boundary layer thickness on the bottom surface of the flap.

The method of calculating boundary layer thickness used was from reference 15. The characteristic length used L was the distance between the impingement of the jet on the flap (stagnation point) and the trailing edge. By referring to figure 29, it can be verified that the nearest high-pressure contour (1.08) of the approach flap setting at approach power (fig. 29(a)) was only about 23 cm (9 in.) from the center of the trailing edge. Likewise for the takeoff flap at takeoff power (fig. 29(b)), the nearest high-pressure contour (1.06) was only about 61 cm (24 in.)from the center of the trailing edge. Using these values for L yielded boundary layer thicknesses of 0.48 cm (0.19 in.) for the approach case and 0.75 cm (0.30 in.) for the takeoff case. Both of these values are remarkably close to the scaled-up model data from reference 14 and the full-scale experimental results.

## SUMMARY OF RESULTS

Test of the under-the-wing (UTW) engine in the Quiet, Clean, Short-Haul Experimental Engine (QCSEE) program yielded the following results:

1. For the approach flap setting at takeoff power the maximum flap surface temperature was 668° R (208° F). For the takeoff flap setting at takeoff power the maximum flap surface temperature was 586° R (126° F).
2. At takeoff power the peak velocity of the QCSEE UTW core nozzle was 261 m/sec. At approach power the peak velocity was 209 m/sec.
3. Flow did not separate from the top surface of the flap at either the takeoff or approach flap setting.
4. For the approach flap setting at approach power the maximum velocity was measured at the trailing edge of the flap. The flow impacted about midchord of the flap and then reorganized and flowed over the surface in the form of a wall jet. For the takeoff flap setting at takeoff power the maximum velocity occurred at a distance of 50 cm (20 in.) below the flap trailing edge. Thus for the takeoff setting, instead of flow impacting on the flap, the jet exhaust flow was turned by the wing-flap system.
5. Boundary layer thicknesses calculated by using a characteristic length equal to the distance from the flow stagnation or impingement point on the flap to the trailing edge agreed with the experimental data.
6. Comparison of spanwise velocity profiles to scaled-model data was good even though the exhaust nozzle used in the model test was a single convergent design.

# APPENDIX A

## METHODS OF CALCULATION

The mass-averaged effective exhaust velocity was calculated from

$$V_e/\sqrt{\theta} = \frac{V_f/\sqrt{\theta}\,(BPR) + V_c/\sqrt{\theta}}{1 + BPR} \tag{A1}$$

and mass-averaged effective temperature from

$$T_e/\sqrt{\theta} = \frac{T_f/\sqrt{\theta}(BPR) + T_c/\sqrt{\theta}}{1 + BPR} \tag{A2}$$

The effective Jet Mach number was calculated from

$$M_{j,e} = \frac{V_e}{\sqrt{\gamma g R T_e}} \tag{A3}$$

The magnitudes of the turbulent boundary layer thickness $\delta$ were determined by fitting the following expression for the logarithmic velocity distribution law to the measured velocity profile data:

$$\frac{U}{U_e}\sqrt{\frac{1}{C_f'}} = 4.137 \log \frac{yU_e\sqrt{C_f'}}{\nu(1.4142)} + 3.932 \tag{A4}$$

This expression represents the universal velocity distribution law presented in reference 15 for flow at very large Reynolds numbers along a flat plate, where $C_f'$ represents the local skin friction coefficient and $U_e$ the local velocity of the flow at the edge of the boundary layer $\delta$. Since the magnitudes of local skin friction coefficients were unknown in the present tests, they were estimated by fitting equation (A4) to the measured velocity distributions. Upon optimization of this procedure, the boundary layer thicknesses $\delta$ were estimated by assuming that the velocity distribution $U/U_e$ reached 0.99 at the edge of the boundary layers. Substitution of 0.99 into equation (A4) resulted in

$$\sqrt{\frac{1}{C_f'}} = 4.179 \log \frac{\delta U_e\sqrt{C_f'}}{\nu(1.4142)} + 3.972 \tag{A5}$$

## APPENDIX B

## SYMBOLS

| | |
|---|---|
| $A_{18}$ | nominal exhaust nozzle area of bypass fan flow (table VI), $m^2$ ($in^2$) |
| BPR | bypass ratio of total fan flow divided by total core flow (table VI) |
| C | chord length (sketch with tables III, IV, and V), m (in.) |
| $C_f'$ | local skin friction coefficient |
| D | diameter of open fan exhaust nozzle (fig. 3), 1.9 m |
| $G_f$ | gap between vane and flap (fig. 4(b)), cm (in.) |
| $G_v$ | gap between wing and vane (fig. 4(b)), cm (in.) |
| g | acceleration due to gravity, 980.7 $cm/sec^2$ (32.174 $ft/sec^2$) |
| LER | leading-edge radius (sketch with table III), cm (in.) |
| $\ell$ | characteristic length (fig. 32), cm (in.) |
| $M_j$ | jet Mach number |
| $M_{j,e}$ | effective jet Mach number (eq. (A3)) |
| $N_f$ | fan speed, rpm |
| $O_f$ | overlap of flap (fig. 4(b)), cm (in.) |
| $O_v$ | overlap of vane (fig. 4(b)), cm (in.) |
| P | measured surface static pressure, $N/cm^2$ (psi) |
| $P_0$ | ambient static pressure, $N/cm^2$ (psi) |
| R | gas constant, evaluated at appropriate temperature and gas composition, J/g K (ft/°R). R = 0.2871 J/g K (53.35 ft/°R) for air near ambient temperature |
| T | measured surface temperature, K (°R) |
| $T_c$ | total core stream temperature, K (°R) |
| $T_e$ | mass-averaged effective temperature (eq. (A2)), K (°R) |
| $T_f$ | mass fan stream temperature, K (°R) |
| $T_N$ | maximum total temperature measured at station 1 during a probe traverse (nozzle exit plane) (fig. 6) |
| $T_0$ | ambient temperature, K (°R) |
| U | mean flow velocity, m/sec (ft/sec) |
| $U_e$ | local mean flow velocity at edge of boundary layer, m/sec (ft/sec) |
| $U_m$ | mean velocity of free shear layer at edge of boundary layer, m/sec (ft/sec) |
| V | velocity, m/sec (ft/sec) |
| $V_c$ | core nozzle exit velocity, m/sec (ft/sec) |
| $V_e$ | effective velocity (eq. (A1)), m/sec (ft/sec) |
| $V_f$ | fan nozzle exit velocity, m/sec (ft/sec) |
| X | distance from fan exhaust exit plane to wing flaps measured along engine centerline, cm (in.) |
| x | distance along chord from leading edge (sketch with table III), cm (in.) |
| Y | spanwise distance, cm (in.) |
| y | vertical distance from chord line to airfoil surface (sketch with table III), cm (in.); normal distance from surface (eq. (A4)) |
| $y_u$ | vertical distance from chord line to upper airfoil surface (sketch with table III), cm (in.) |
| $y_\ell$ | vertical distance from chord line to lower airfoil surface (sketch with table III), cm (in.) |
| x,y,z | Cartesian coordinate system (fig. 24) |
| Z | vertical distance above or below flap, cm (in.) |
| $\beta_f$ | fan blade angle from design forward blade angle (table VI), deg |

| | |
|---|---|
| $\gamma$ | ratio of specific heats, evaluated at appropriate temperature and gas composition, dimensionless. $\gamma = 1.4$ for air near ambient temperature |
| $\delta$ | thickness of boundary layer, cm (in.) |
| $\nu$ | kinematic viscosity, $m^2/sec$ ($ft^2/sec$) |
| $\theta$ | ratio of total temperature to standard-day temperature, dimensionless. $\theta = T/288.2$ K ($T/518.7^\circ$ R) |
| $\psi_f$ | angle between chord line of wing and chord line of flap (table VI), deg |
| $\psi_v$ | angle between chord line of wing and chord line of vane (table VI), deg |

Subscripts:

| | |
|---|---|
| c | chord or core |
| f | flap or fan |
| v | vane |
| w | wing |

## REFERENCES


1. Ciepluch, C. C.: A Review of the QCSEE Program. NASA TM X-71818, 1975.
2. Ciepluch, C. C.: Overview of the QCSEE Program. Powered-Lift Aerodynamics and Acoustics, NASA SP-406, 1976, pp. 325-333.
3. Quiet, Clean, Short-Haul Experimental Engine QCSEE Under the Wing (UTW). NASA CR-134847, 1977.
4. Stimpert, D. L.: Quiet, Clean, Short-Haul Experimental Engine QCSEE Under the Wing (UTW) Composite Nacelle Test Report. Vol. 2: Acoustic Performance. (R78AEG574-Vol-2, General Electric Corp; NAS3-18021.) NASA CR-159472, 1979.
5. Bloomer, H. E.; and Samanich, N. E.: QCSEE Fan Exhaust Bulk Absorber Treatment Evaluation. AIAA Paper 80-0987, June 1980.
6. Loeffler, I. J.; Samanich, N. E.; and Bloomer, H. E.: QCSEE UTW Engine Powered-Lift Acoustic Performance. AIAA Paper 80-1065, June 1980.
7. Bloomer, H. E.; et al.: Comparison of NASA and Contractor Results from Tests of QCSEE OTW Engine. NASA TM-81761, 1981.
8. Clemons, A.: Quiet, Clean, Short-Haul Experimental Engine (QCSEE): Acoustic Treatment Development and Design. (R76AEG379-1, General Electric Co.; NAS3-18021.) NASA CR-135266, 1979.
9. Loeffler, I. J.; Smith, E. B.; and Sowers, H. D.: Acoustic Design of the QCSEE Propulsion Systems. Powered-Lift Aerodynamics and Acoustics, NASA SP-406, 1976, pp. 335-356.
10. Quiet, Clean, Short-Haul Experimental Engine (QCSEE) - Under the Wing Engine Digital Control System Design Report. (R75AEG483, General Electric Corp.; NAS3-18021.) NASA CR-134920, 1978.
11. Bloomer, H. E.; and Samanich, N. E.: QCSEE Under-the-Wing Acoustic Data Report. NASA TM-82691, 1982.
12. Whitcomb, R. T.: Review of NASA Supercritical Airfoils. ICAS Paper 74-10, Aug. 1974.
13. Gettleman, C. C.; and Krause, L. N.: Considerations Entering into the Selection of Probes for Pressure Measurement in Jet Engines. Paper 52-12-1, ISA Proceedings, Vol. 7, 1952, pp. 134-137.
14. McKinzie, D. J., Jr.: Measured and Predicted Impingment Noise for a Model Scale Under-the-Wing Externally Blown Flap Configuration with a QCSEE-Type Nozzle. NASA TM-81494, 1980.
15. Renshaw, J. H.: Quiet Turbofan STOL Aircraft for Short Haul Transportation. NASA CR-114612, 1973.
16. Burns, R. J.; McKinzie, D. J., Jr.; and Wagner, J. M.: Effects of Perforated Flap Surfaces and Screens on Acoustics of a Large Externally Blown Flap Model. NASA TM X-3335, 1976.
17. Schlichting, H.: Boundary Layer Theory. 1st ed., Pergamon Press, 1955, p. 437.

TABLE I. - ENGINE DESIGN PARAMETERS FOR QCSEE UTW ENGINE

[41.2-m/sec (80-knot) aircraft speed; 61-m (200-ft) altitude; takeoff conditions.]

| | |
|---|---|
| Number of fan blades | 18 |
| Fan diameter, $D_F$, cm (in.) | 180.4 (71) |
| Fan pressure ratio | 1.27 |
| Fan speed, rpm | 3089 (3244 at 100%) |
| Fan tip speed, m/sec (ft/sec) | 289.6 (950) |
| Number of outlet guide vanes | 33 (32 + pylon) |
| Fan weight flow (corrected), kg/sec (lbm/sec) | 405.5 (894) |
| Inlet Mach number (throat) | 0.79 |
| Rotor OGV spacing, rotor tip aerodynamic chords | 1.5 |
| Fan exhaust area, $m^2$ ($in^2$) | 1.615 (2504) |
| Core exhaust area, $m^2$ ($in^2$) | 0.348 (540) |
| Gross thrust (sea-level static uninstalled), kN (lb) | 81.39 (18 300) |
| Blade passing frequency, Hz | 927 |
| Core exhaust flow, kg/sec (lbm/sec) | 31.3 (69.1) |
| Fan exhaust velocity, m/sec (ft/sec) | 197.8 (649) |
| Core exhaust velocity, m/sec (ft/sec) | 238.9 (784) |
| Bypass ratio | 12.1 |
| Ratio of inlet treatment length to fan diameter, $L_T/D_F$ | 0.74 |
| Vane-blade ratio | 1.83 |

TABLE II. - NOMINAL QCSEE UTW ENGINE CONDITIONS (AS TESTED)

| Condition | Takeoff | Approach |
|---|---|---|
| Corrected fan speed, percent | 95 | 95 |
| Fan exhaust area, $m^2$ ($in^2$) | 1.516 (2350) | 1.870 (2900) |
| Core exhaust area, $m^2$ ($in^2$) | 0.348 (540) | 0.348 (540) |
| Fan blade angle (panel + 28°), deg | -7.6 | +5.2 |
| Corrected gross thrust (installed), kN (lbf) | 77.39 (17 400) | 55.42 (12 460) |
| Inlet throat Mach number (one dimensional) | 0.79 | 0.63 |
| Fan pressure ratio | 1.25 | 1.14 |
| Bypass ratio | 11.7 | 12.9 |
| Fan exhaust velocity, m/sec (ft/sec) | 195 (640) | 151 (495) |
| Core exhaust velocity, m/sec (ft/sec) | 253 (830) | 177 (580) |
| Mass average velocity, m/sec (ft/sec) | 200 (655) | 152 (500) |

TABLE III. - QCSEE UTW ENGINE WING AIRFOIL COORDINATES ALONG STREAMWISE CHORDS

[LER/c = 0.0428; $(x/C)_{LER}$ = 0.0427; $(y/C)_{LER}$ = 0.]

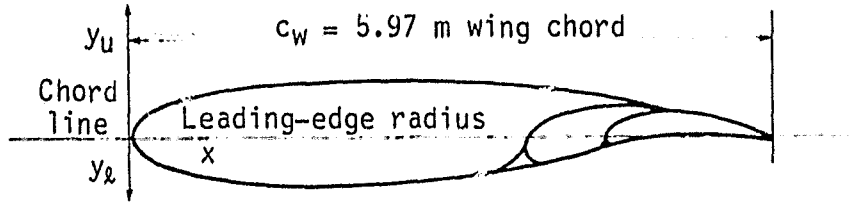


| Ratio of distance along chord from leading edge to wing chord, $x/C_w$ | Ratio of vertical distance from chord line to airfoil surface | |
|---|---|---|
| | $y_u/C_w$ | $y_\ell/C_w$ |
| 0.0125 | 0.0292 | 0.0312 |
| .0250 | .0397 | .0414 |
| .0375 | .0464 | .0482 |
| .0500 | .0542 | .0534 |
| .0750 | .0591 | .0606 |
| .1000 | .0648 | .0658 |
| .1250 | .0694 | .0700 |
| .1500 | .0733 | .0730 |
| .1750 | .0766 | .0756 |
| .2000 | .0792 | .0777 |
| .2500 | .0831 | .0804 |
| .3000 | .0861 | .0818 |
| .3500 | .0880 | .0816 |
| .4000 | .0892 | .0805 |
| .4500 | .0894 | .0780 |
| .5000 | .0885 | .0737 |
| .5500 | .0865 | .0675 |
| .5750 | .0852 | .0634 |
| .6000 | .0834 | .0587 |
| .6250 | .0815 | .0533 |
| .6500 | .0791 | .0477 |
| .6750 | .0765 | .0419 |
| .7000 | .0736 | .0359 |
| .7250 | .0696 | .0299 |
| .7500 | .0654 | .0239 |
| .7750 | .0612 | .0183 |
| .8000 | .0561 | .0156 |
| .8250 | .0504 | .0087 |
| .8500 | .0443 | .0052 |
| .8750 | .0376 | .0030 |
| .9000 | .0314 | .0013 |
| .9250 | .0237 | .0012 |
| .9500 | .0162 | .0022 |
| .9750 | .0239 | .0045 |
| 1.0000 | 0 | .0077 |

TABLE IV. - QCSEE UTW ENGINE VANE COORDINATES

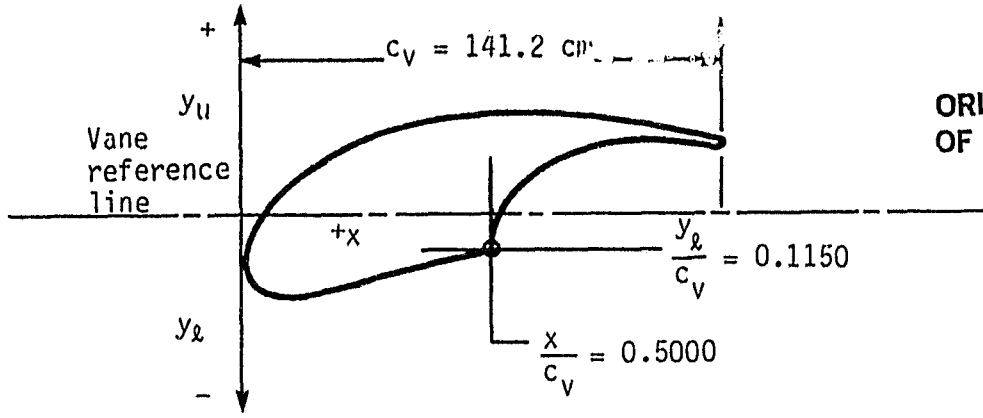




| Distance along chord from leading edge, x | Vertical distance from chord line to airfoil upper surface, $y_u$ | Vertical distance from chord line to airfoil lower surface, $y_\ell$ |
|---|---|---|
| Percent of chord | | |
| 0 | -12.50 | -12.50 |
| 1.25 | -6.52 | -16.50 |
| 2.50 | -4.00 | -18.09 |
| 5.00 | -.30 | -19.49 |
| 7.50 | 3.55 | -20.20 |
| 10.00 | 4.82 | -20.48 |
| 15 | 8.50 | -20.13 |
| 20 | 11.52 | -19.19 |
| 25 | 14.10 | -17.98 |
| 30 | 16.28 | -16.51 |
| 35 | 18.01 | -15.13 |
| 40 | 19.40 | -13.82 |
| 45 | 20.39 | -12.60 |
| 50 | 21.05 | -11.50 |
| 51.25 | ------ | -.60 |
| 52.50 | ------ | 2.00 |
| 53.75 | ------ | 3.80 |
| 55 | 21.50 | 5.10 |
| 60 | 21.84 | 9.98 |
| 65 | 21.93 | 11.60 |
| 70 | 21.82 | 13.50 |
| 75 | 21.51 | 14.90 |
| 80 | 21.13 | 15.85 |
| 85 | 20.61 | 16.38 |
| 90 | 19.91 | 16.71 |
| 95 | 19.09 | 16.75 |
| 100 | 18.00 | 16.55 |

TABLE V. - QCSEE UTW ENGINE FLAP COORDINATES

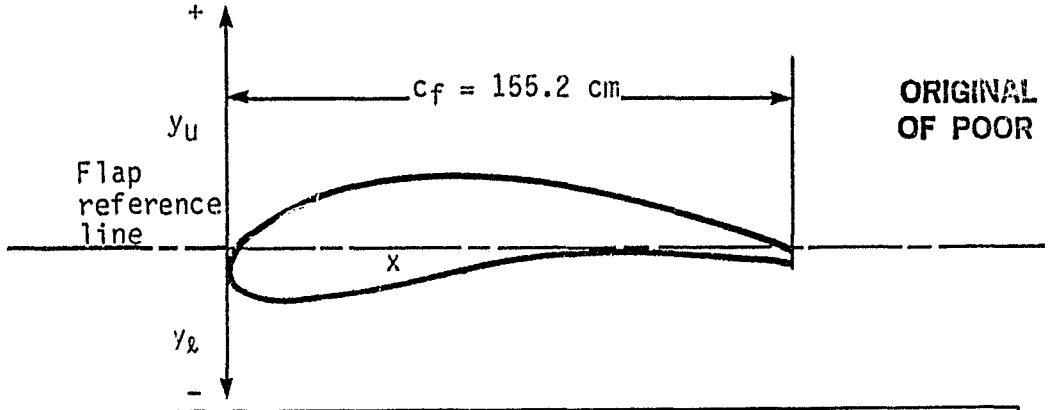




| Distance along chord from leading edge, x | Vertical distance from chord line to airfoil upper surface, $y_u$ | Vertical distance from chord line to airfoil lower surface, $y_\ell$ |
|---|---|---|
| Percent of chord | | |
| 0 | -4.00 | -4.00 |
| 1.25 | -7.00 | 7.38 |
| 2.50 | -1.92 | 8.42 |
| 5.00 | 4.79 | 8.70 |
| 7.50 | 6.93 | 8.45 |
| 10 | 8.68 | 7.87 |
| 15 | 11.01 | 6.70 |
| 20 | 12.64 | 5.64 |
| 25 | 13.78 | 4.67 |
| 30 | 14.52 | 3.75 |
| 35 | 14.98 | 2.90 |
| 40 | 15.06 | 2.15 |
| 45 | 14.83 | 1.52 |
| 50 | 14.25 | 1.02 |
| 55 | 13.38 | .66 |
| 60 | 12.32 | .43 |
| 65 | 11.12 | .37 |
| 70 | 9.75 | .46 |
| 75 | 8.26 | .68 |
| 80 | 6.68 | 1.00 |
| 85 | 5.00 | 1.37 |
| 90 | 3.25 | 1.79 |
| 95 | 1.41 | 2.24 |
| 100 | -.43 | 2.70 |

TABLE VI. - CONDITIONS FOR UTW ENGINE-WING-FLAP AERODYNAMIC PROFILE DATA

| Engine setting | Run | Nominal fan speed, $N_F$, percent of rated | Rake position code | Nominal exhaust nozzle area, $A_{18}$ | | Nominal fan blade angle, $\beta_f$, deg | Wing flap setting, $\phi_v/\phi_f$, deg | Exhaust nozzle traversing probe data | Fan nozzle exit velocity, $V_f$ | | Core nozzle exit velocity, $V_c$ | | Mass-averaged effective velocity, $V_e$ | | Bypass ratio, BPR | Core exhaust gas temperature, $T_c$, °R | Fan stream temperature, $T_f$, °R | Mass-weighted average temperature, $T_e$, °R | Effective jet Mach number, $M_{j,e}$ |
|---|---|---|---|---|---|---|---|---|---|---|---|---|---|---|---|---|---|---|---|
| | | | | $m^2$ | $in^2$ | | | | m/sec | ft/sec | m/sec | ft/sec | m/sec | ft/sec | | | | | |
| Approach | 4 | 95 | 1A,2A,3A | 1.87 | 2900 | +5.2 | 30/60 | (a) | 156.4 | 513 | 186.5 | 612 | 161.3 | 529.2 | 12.9 | 1596 | 580 | 653 | 0.427 |
| | 5 | 81 | | 1.49 | 2310 | -7.6 | | | 173.1 | 568 | 192.9 | 633 | 177.9 | 583.5 | 12.0 | 1631 | 556 | 639 | .474 |
| | 6 | 85 | | | | | | | 183.8 | 603 | 213.3 | 700 | 189.5 | 621.8 | 11.9 | 1674 | 564 | 651 | .501 |
| | 7 | 90 | | | | | | | 196.9 | 646 | 243.2 | 798 | 204.2 | 670.1 | 11.7 | 1738 | 572 | 665 | .534 |
| Takeoff | 8 | 94 | | | | | | | 211.5 | 694 | 280.4 | 920 | 221.2 | 725.8 | 11.4 | 1811 | 583 | 682 | .572 |
| Approach | 10 | 95 | 1A,2B,3B | 1.87 | 2900 | +5.2 | | | 156.4 | 513 | 186.5 | 612 | 160.3 | 525.8 | 12.9 | 1596 | 580 | 653 | .423 |
| | 11 | 81 | | 1.49 | 2310 | -7.6 | | | 173.1 | 568 | 192.9 | 633 | 176.6 | 579.3 | 12.0 | 1631 | 556 | 639 | .471 |
| | 12 | 85 | | | | | | | 183.2 | 603 | 213.3 | 700 | 188.2 | 617.3 | 11.9 | 1674 | 564 | 651 | .497 |
| | 13 | 90 | | | | | | | 196.9 | 646 | 243.2 | 798 | 202.8 | 665.3 | 11.7 | 1738 | 572 | 665 | .530 |
| Takeoff | 14 | 94 | | | | | | | 211.5 | 694 | 280.4 | 920 | 219.6 | 720.4 | 11.4 | 1811 | 583 | 682 | .568 |
| | 18 | 81 | 1A,2B,3B | | | | 12/18 | Yes | 176.8 | 580 | 196.6 | 645 | 182.1 | 597.4 | 12.0 | 1631 | 556 | 639 | .486 |
| | 19 | 85 | | | | | | | 185.0 | 607 | 217.9 | 715 | 191.3 | 627.7 | 11.8 | 1674 | 564 | 651 | .505 |
| | 20 | 90 | | | | | | | 199.6 | 655 | 252.4 | 828 | 207.8 | 681.9 | 11.6 | 1738 | 572 | 665 | .543 |
| | 21 | 94 | | | | | | | 211.5 | 694 | 280.4 | 920 | 221.5 | 726.8 | 11.4 | 1811 | 583 | 682 | .572 |
| | 22 | 95 | | 1.54 | 2390 | | | | 201.2 | 660 | 269.7 | 885 | 211.0 | 692.3 | 11.6 | 1811 | 583 | 680 | .546 |
| Approach | 23 | 95 | | 1.87 | 2900 | +5.2 | | | 156.4 | 513 | 186.5 | 612 | 161.8 | 530.9 | 12.9 | 1596 | 580 | 653 | .427 |
| Takeoff | 24 | 94 | 1A,2A,3A | 1.49 | 2310 | -7.6 | | No | 211.5 | 694 | 280.4 | 920 | 222.5 | 729.9 | 11.4 | 1811 | 583 | 682 | .574 |
| | 25 | 90 | | | | | | | 199.6 | 655 | 252.4 | 828 | 208.8 | 685.0 | 11.6 | 1738 | 572 | 665 | .546 |
| | 26 | 85 | | | | | | | 185.0 | 607 | 217.9 | 715 | 192.2 | 630.6 | 11.8 | 1674 | 564 | 651 | .508 |
| | 27 | 81 | | | | | | | 176.8 | 580 | 196.6 | 645 | 182.6 | 599.0 | 12.0 | 1631 | 556 | 639 | .487 |
| | 28 | 95 | | 1.54 | 2390 | | | | 201.2 | 660 | 269.7 | 885 | 211.7 | 694.4 | 11.6 | 1811 | 583 | 680 | .547 |
| | 29 | 31 | 1A,2D,3D | 1.49 | 2310 | | | | 176.8 | 580 | 196.6 | 645 | 182.8 | 599.9 | 12.0 | 1631 | 556 | 639 | .488 |
| | 30 | 94 | | | | | | | 211.5 | 694 | 280.4 | 920 | 222.9 | 731.2 | 11.4 | 1811 | 583 | 682 | .575 |
| | 31 | 85 | | | | | | | 185.0 | 607 | 217.9 | 715 | 192.5 | 631.4 | 11.8 | 1674 | 564 | 651 | .508 |
| | 32 | 90 | | | | | | | 199.6 | 655 | 252.4 | 828 | 208.7 | 684.8 | 11.6 | 1738 | 572 | 665 | .546 |
| | 33 | 95 | | 1.54 | 2390 | | | | 201.2 | 660 | 269.7 | 885 | 211.9 | 695.8 | 11.6 | 1811 | 583 | 680 | .548 |
| | 34 | 81 | 1A,2C,3C | 1.49 | 2310 | | | | 176.8 | 580 | 196.6 | 645 | 182.1 | 597.6 | 12.0 | 1631 | 556 | 639 | .486 |
| | 35 | 85 | | | | | | | 185.0 | 607 | 217.9 | 715 | 191.6 | 628.7 | 11.8 | 1674 | 564 | 651 | .506 |
| | 36 | 90 | | | | | | | 199.6 | 655 | 252.4 | 828 | 206.7 | 678.2 | 11.6 | 1738 | 572 | 665 | .540 |
| | 37 | 94 | | | | | | | 211.5 | 694 | 280.4 | 920 | 270.2 | 722.3 | 11.4 | 1811 | 583 | 682 | .568 |
| | 38 | 95 | | 1.54 | 2390 | | | | 201.2 | 660 | 269.7 | 885 | 209.5 | 687.4 | 11.6 | 1811 | 583 | 680 | .542 |

[a]Temperature not available.

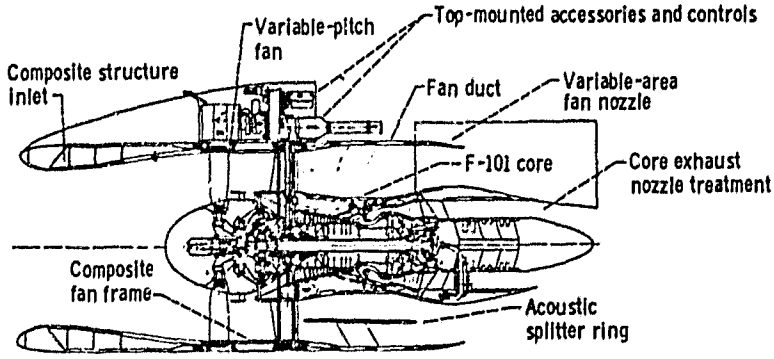


Figure 1. - UTW experimental propulsion system.

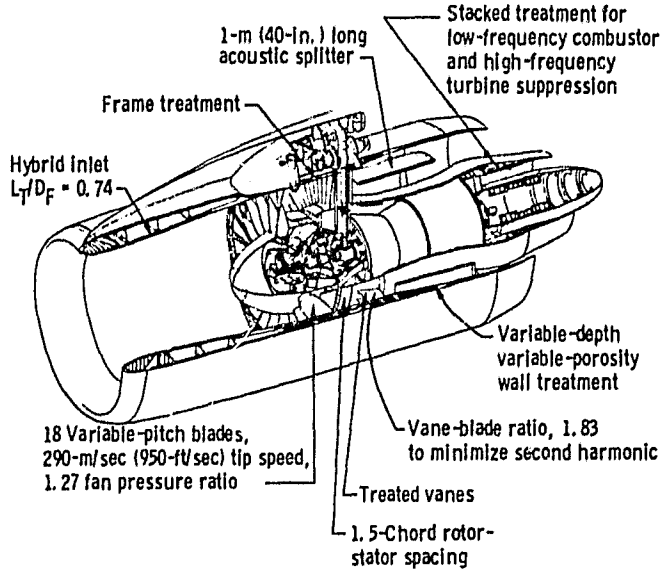


Figure 2. - Acoustic design features of QCSEE UTW engine.

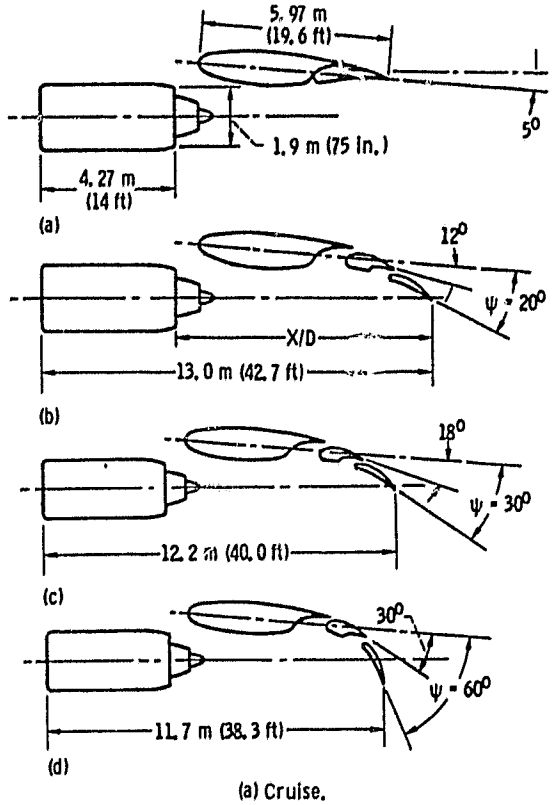


(a) Cruise.
(b) Takeoff, $\psi = 20^{\circ}$.
(c) Takeoff, $\psi = 30^{\circ}$.
(d) Approach, $\psi = 60^{\circ}$.

Figure 3. - UTW wing-flap configurations.

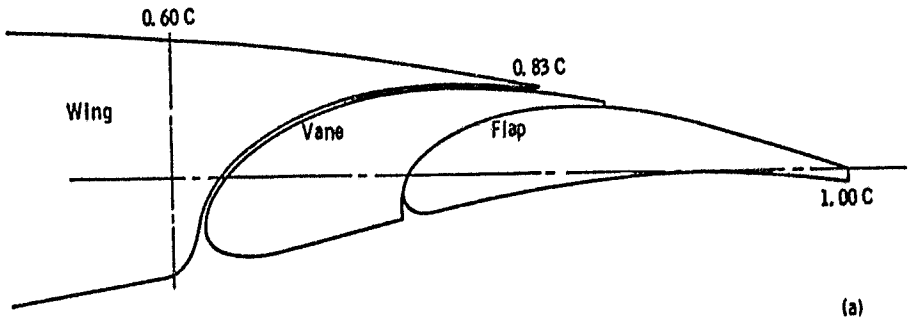


(a)

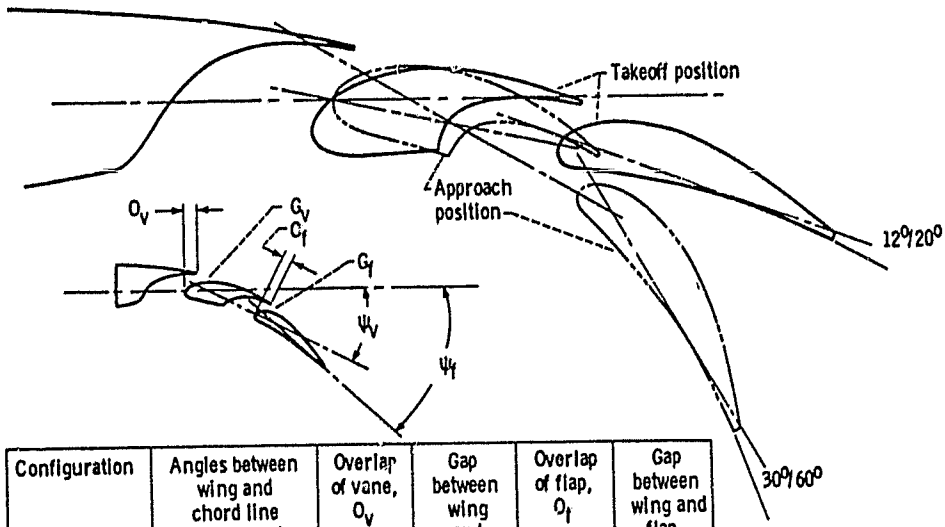


| Configuration | Angles between wing and chord line of vane and flap, $\psi_v / \psi_f$, deg | Overlap of vane, $O_v$ | Gap between wing and vane, $G_v$ | Overlap of flap, $O_f$ | Gap between wing and flap, $G_f$ |
|---|---|---|---|---|---|
| | | Percent of local wing chord | | | |
| Takeoff | 12/20 | 4.00 | 3.00 | 1.42 | 2.25 |
| Approach | 30/60 | 2.00 | 2.50 | 0 | 2.50 |

(b)

(a) In cruise position.
(b) In takeoff and approach positions.

Figure 4. - Details of vane and flap.

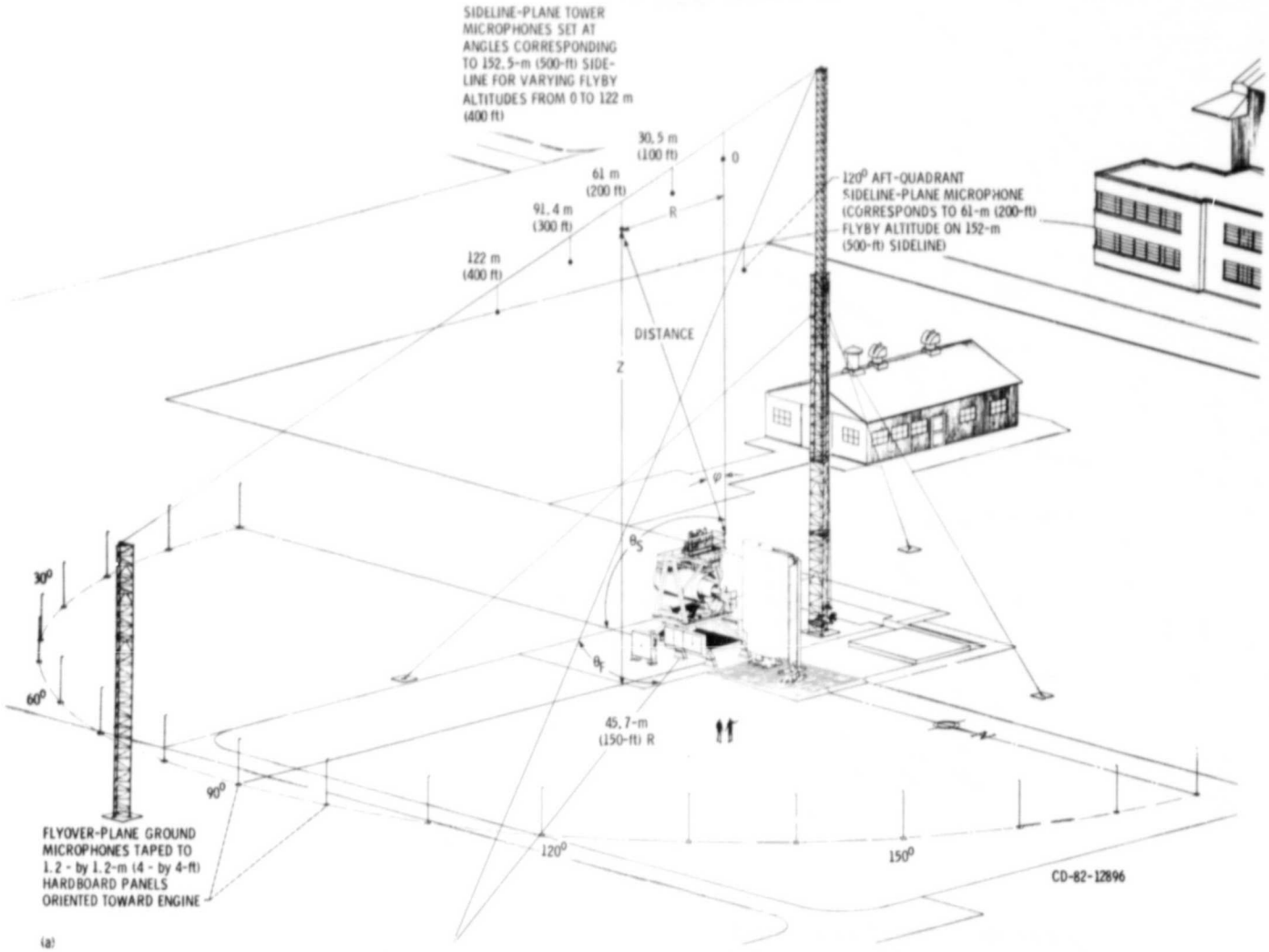


(a)

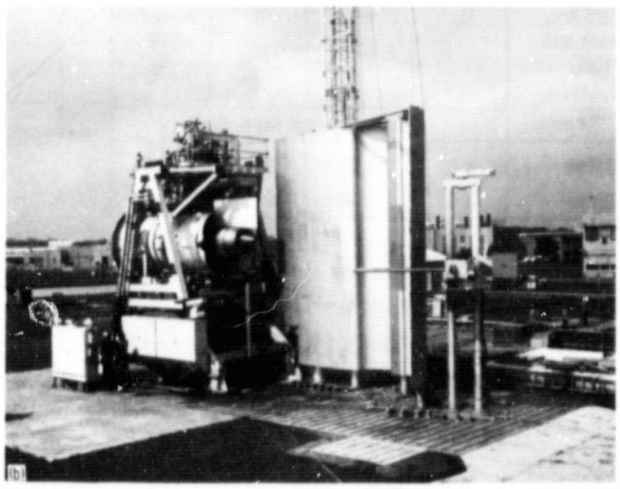

(b)

(a) Sketch showing general layout.

(b) Engine stand and super rake in position B. Exhaust nozzle shown flared out in "reverse thrust" position.

Figure 5. - Engine Noise Test Facility.

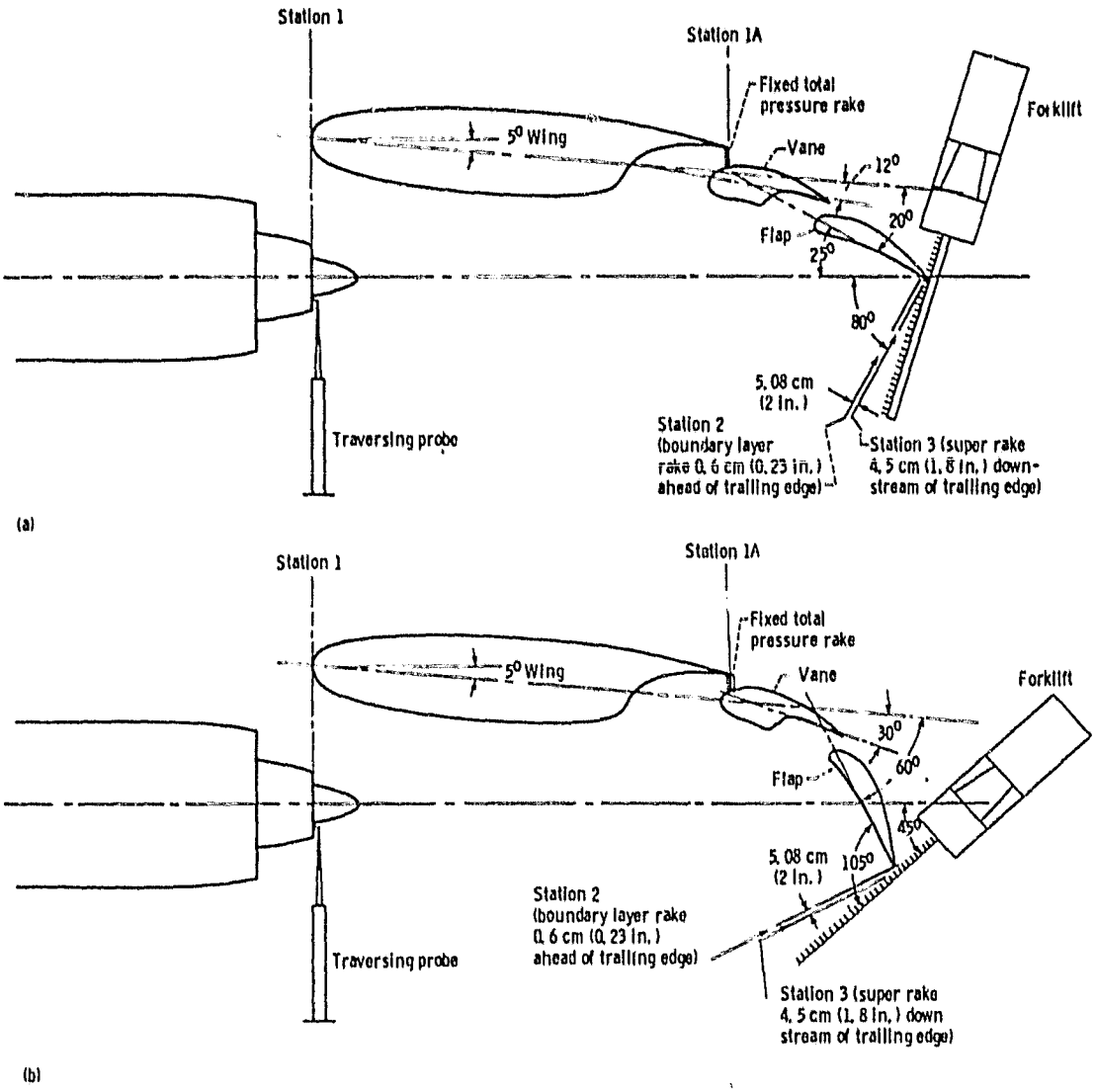


(a) Wing-flap shown in takeoff position.
(b) Wing-flap shown in approach position.

Figure 6. - General arrangement of QCSEE UTW engine flow measurement instrumentation.

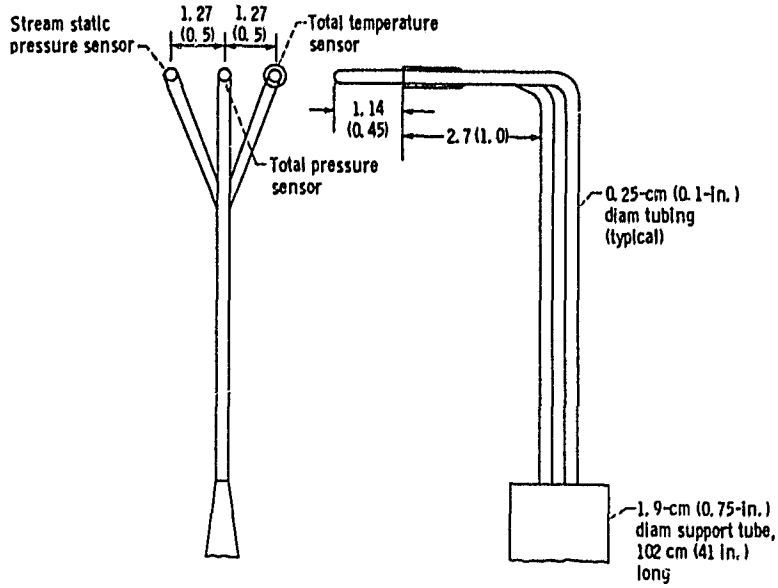


Figure 7. - Total and static pressure and temperature traversing probe for QCSEE UTW engine exhaust survey at station 1. (All dimensions are in centimeters (inches).)

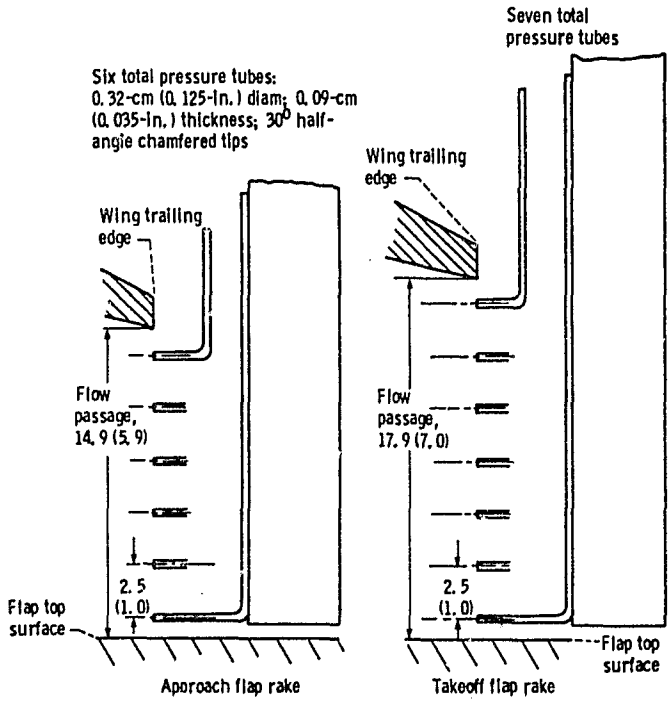


Figure 8. - Station 1A total pressure rakes - set parallel to minimum distance between QCSEE UTW wing trailing edge and flap and centered in flow passage. (All dimensions are in centimeters (inches).)

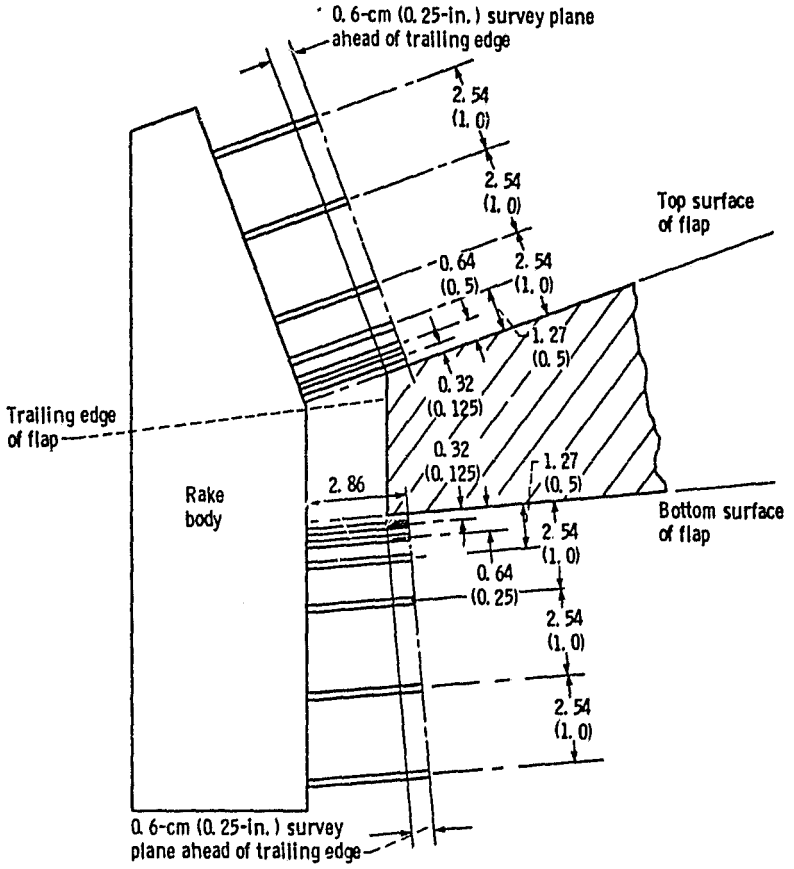


Figure 9. - Station 2 boundary layer rakes - 12 total pressure tubes: 0.163 cm (0.063 in.) diameter; 0.03 cm (0.01 in.) wall thickness; 30° half-angle chamfered tips. (All dimensions are in centimeters (inches).)

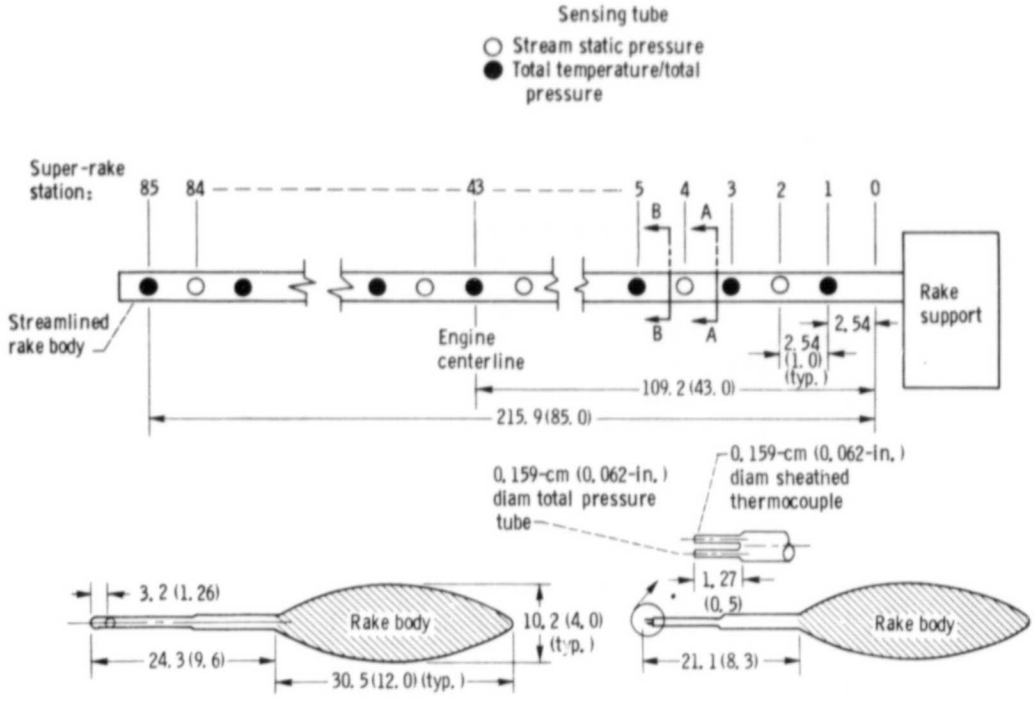


Section A-A: Typical of all stream static pressure sensing tubes (42 tubes total)

Section B-B: Typical of all total temperature/ total pressure sensing tubes (43 pairs total)

(a)


(a) Schematic drawing. (All dimensions are in centimeters (inches)).
(b) Super rake on mounting cart.

Figure 10. - Super rake used for QCSEE UTW flow surveys at station 3.

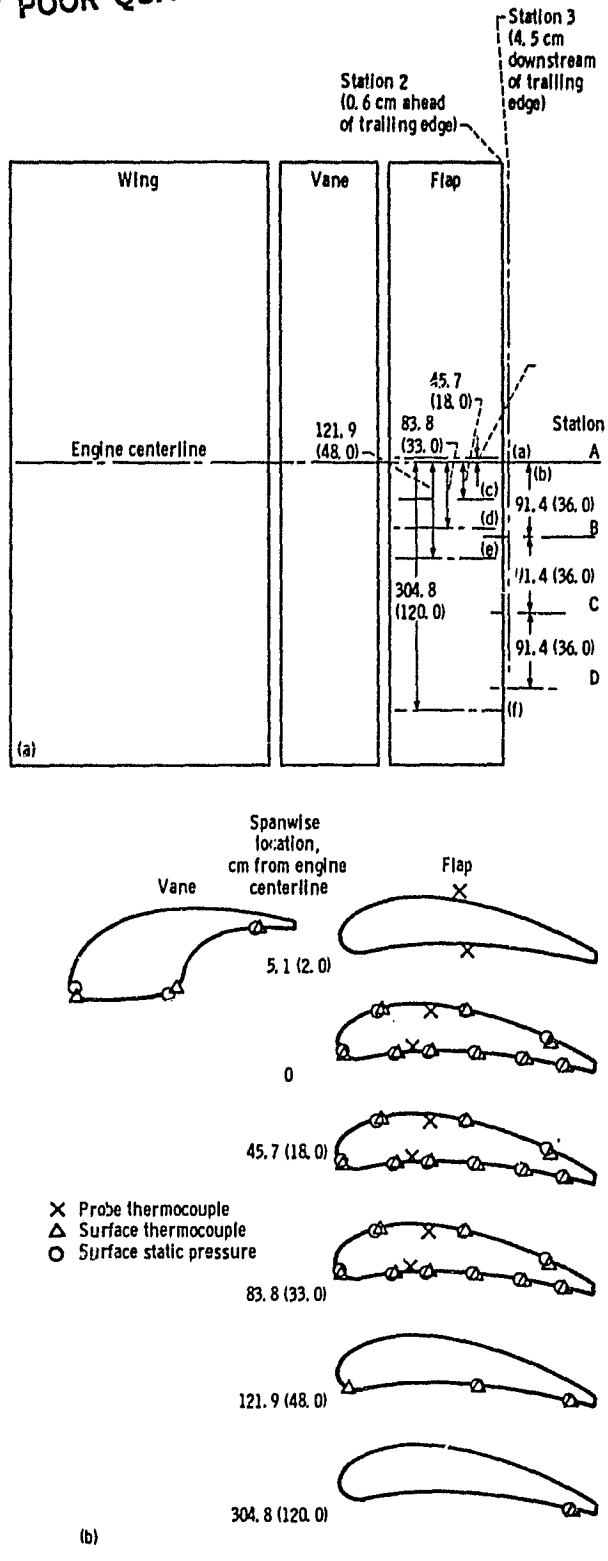


(a) Instrumentation.

(b) Instrumentation detail.

Figure 11. - Schematic of QCSEE UTW wing-flap system showing spanwise locations. (All dimensions are in centimeters (inches).)

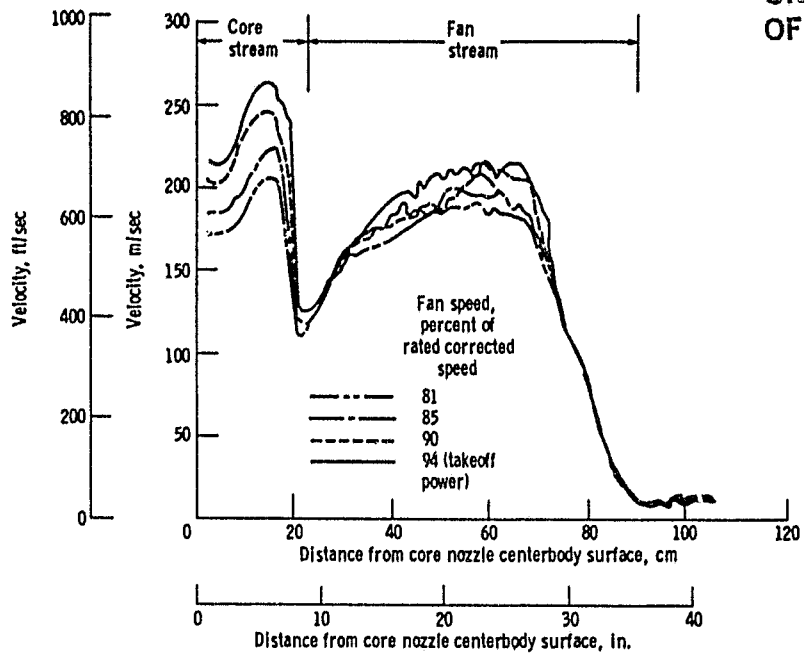


Figure 12. - Effect of fan speed on QCSEE UTW velocity survey at station 1. Exhaust nozzle area, 1.49 $m^2$ (2310 $in^2$); fan blade setting, -7.6°.

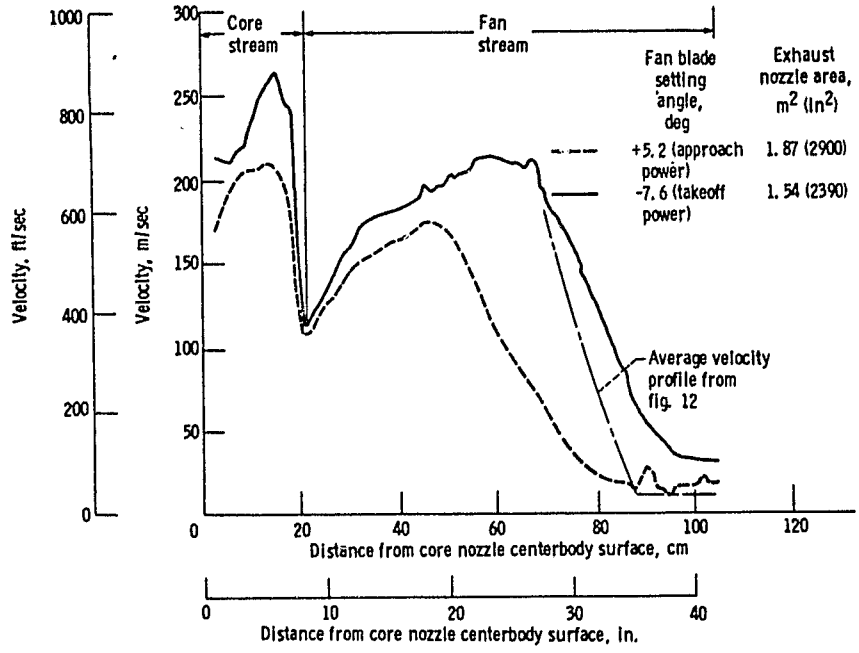


Figure 13. - Effect of exhaust nozzle area and fan blade setting angle on QCSEE UTW velocity survey at station 1. Fan speed, 95 percent of rated corrected speed.

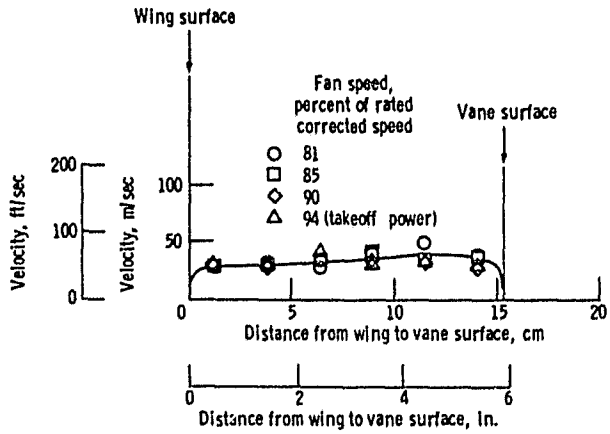


Figure 14. - Effect of fan speed on QCSEE UTW velocity survey at station 1A. Approach flap setting; exhaust nozzle area, 1.49 $m^2$ (2310 $in^2$); fan blade setting angle, -7.6°.

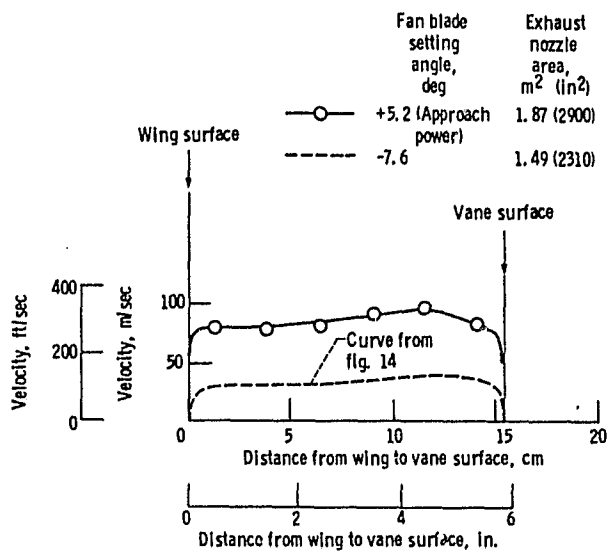


Figure 15. - Effect of exhaust nozzle area and fan blade setting angle on QCSEE UTW velocity survey at station 1A. Approach flap setting; fan speed, 95 percent of rated.

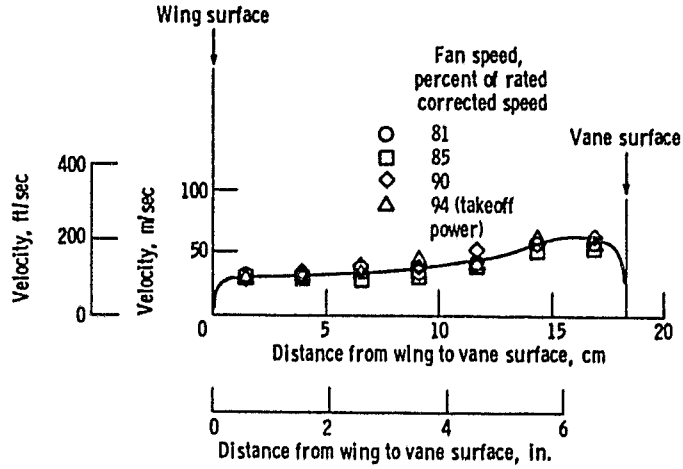


Figure 16. - Effect of fan speed on QCSEE UTW velocity survey at station 1A. Takeoff flap setting; exhaust nozzle area, 1.49 $m^2$ (2310 $in^2$); fan blade setting angle, -7.6°.

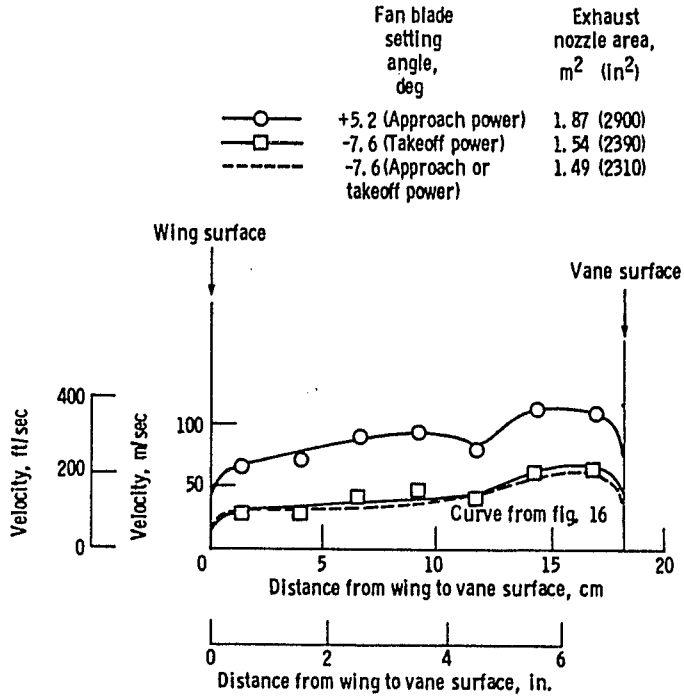


Figure 17. - Effect of exhaust nozzle area and fan blade setting angle on QCSEE UTW velocity survey at station 1A. Takeoff flap setting; fan speed, 95 percent of rated.

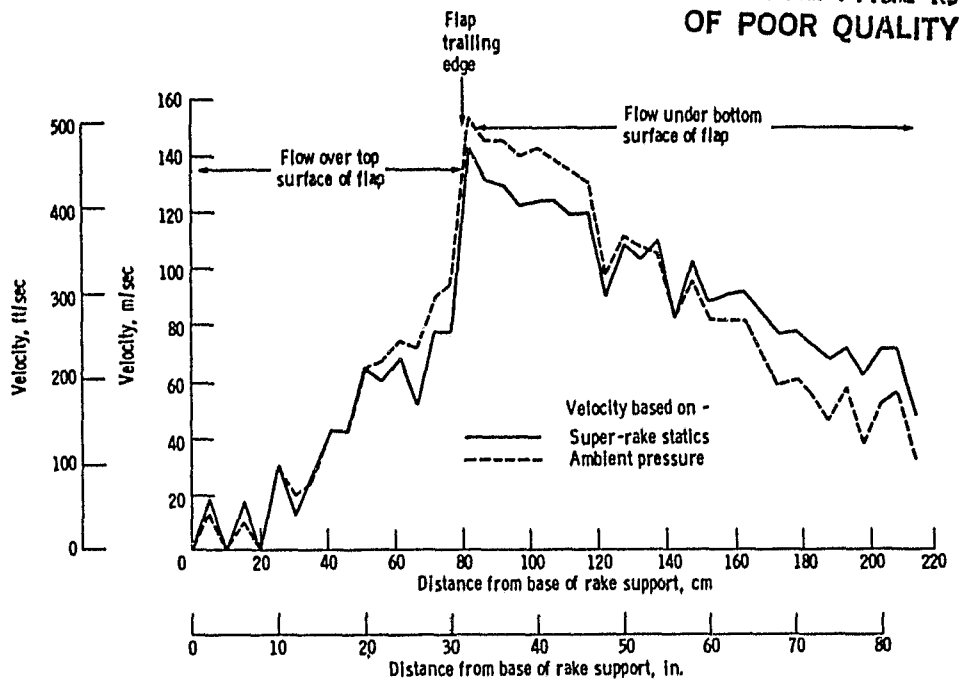


Figure 18. - QCSEE UTW velocity surveys at station 3 and spanwise station A calculated by two different methods - approach flap setting at approach power.

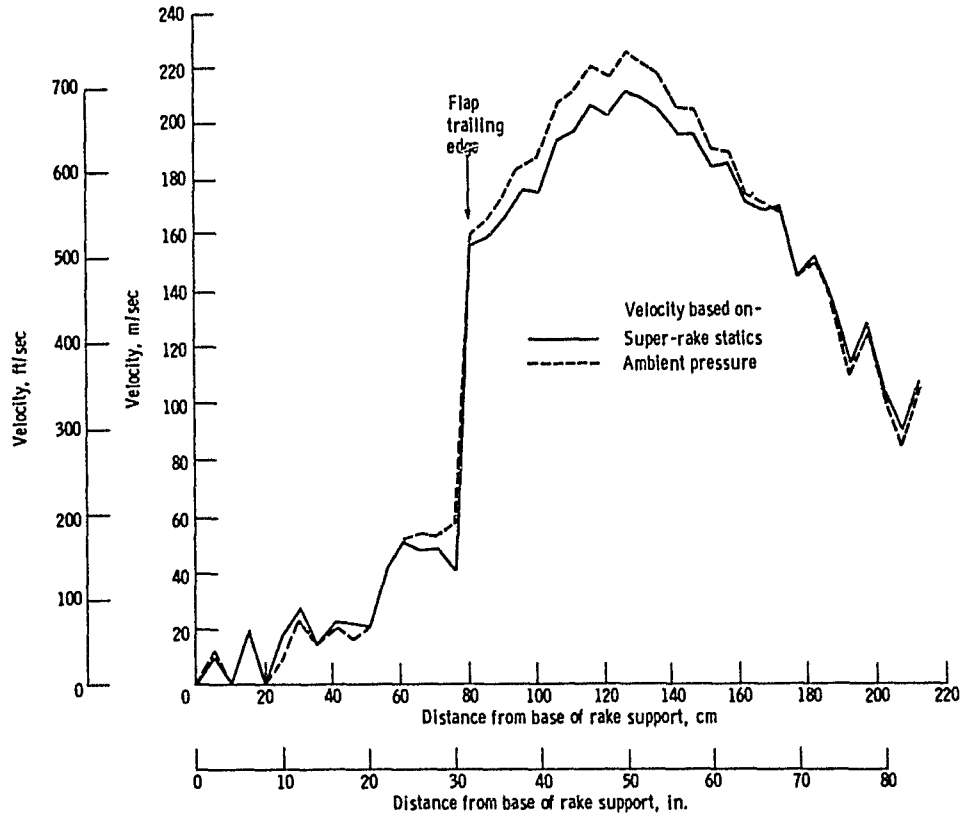


Figure 19. - QCSEE UTW velocity surveys at station 3 and spanwise station A calculated by two different methods - takeoff flap setting at takeoff power.

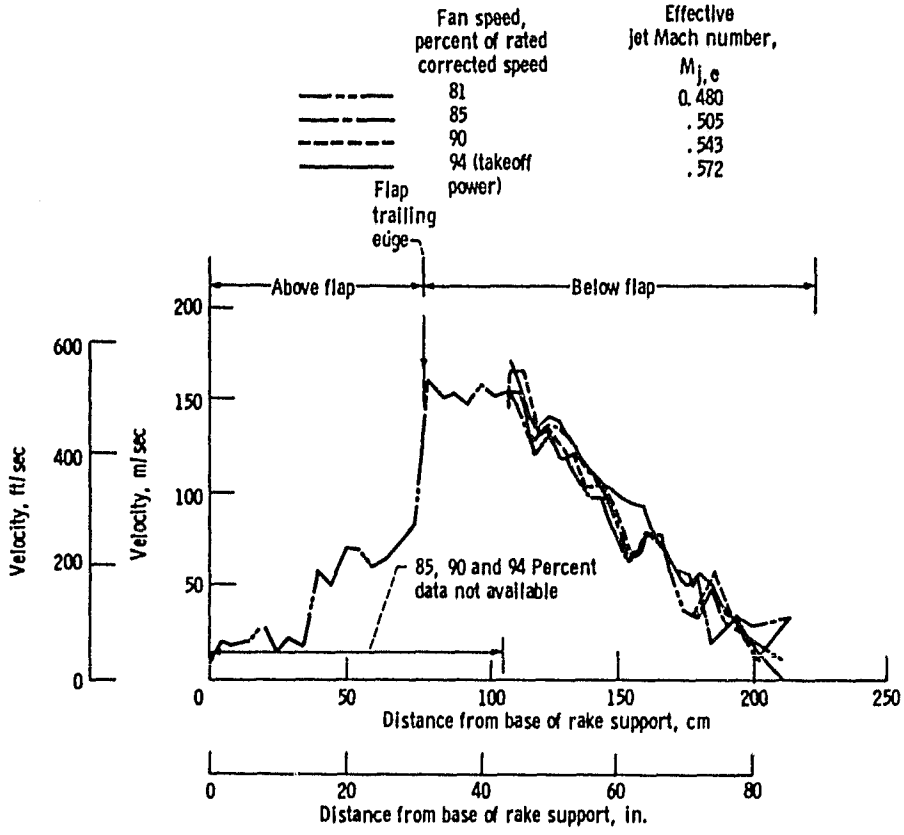


Figure 20. - Effect of fan speed on QCSEE UTW velocity survey at station 3 and spanwise station A - approach flap setting.

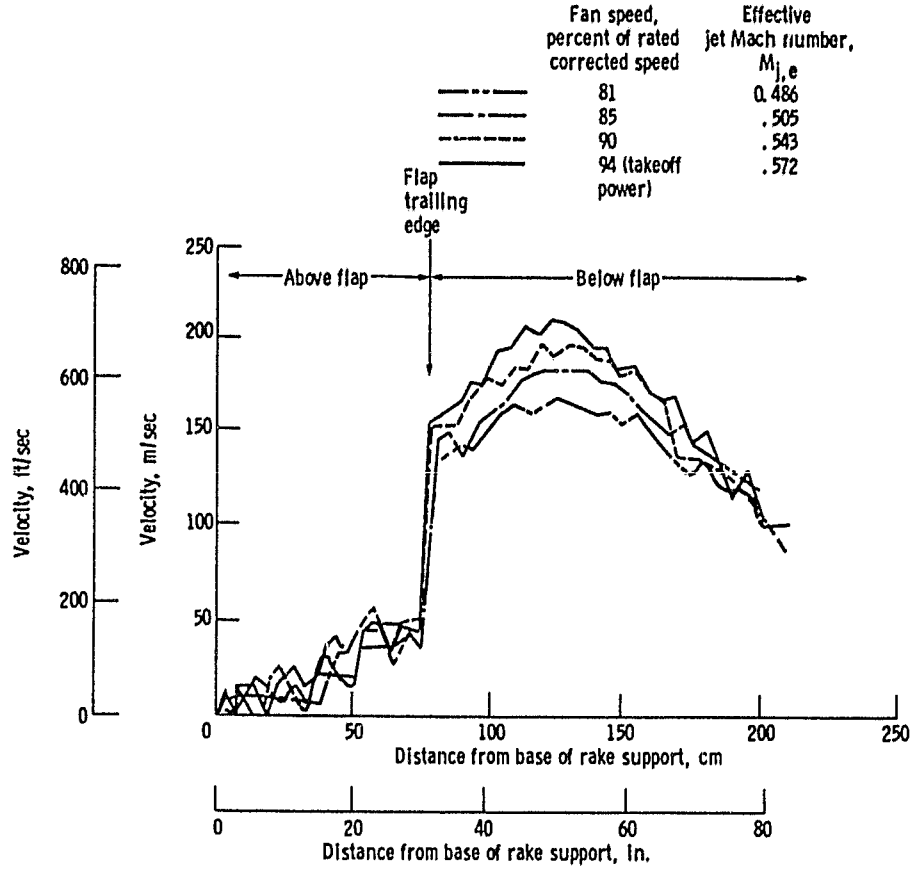


Figure 21. - Effect of fan speed on QCSEE UTW velocity survey at station 3 and spanwise station A - takeoff flap setting.

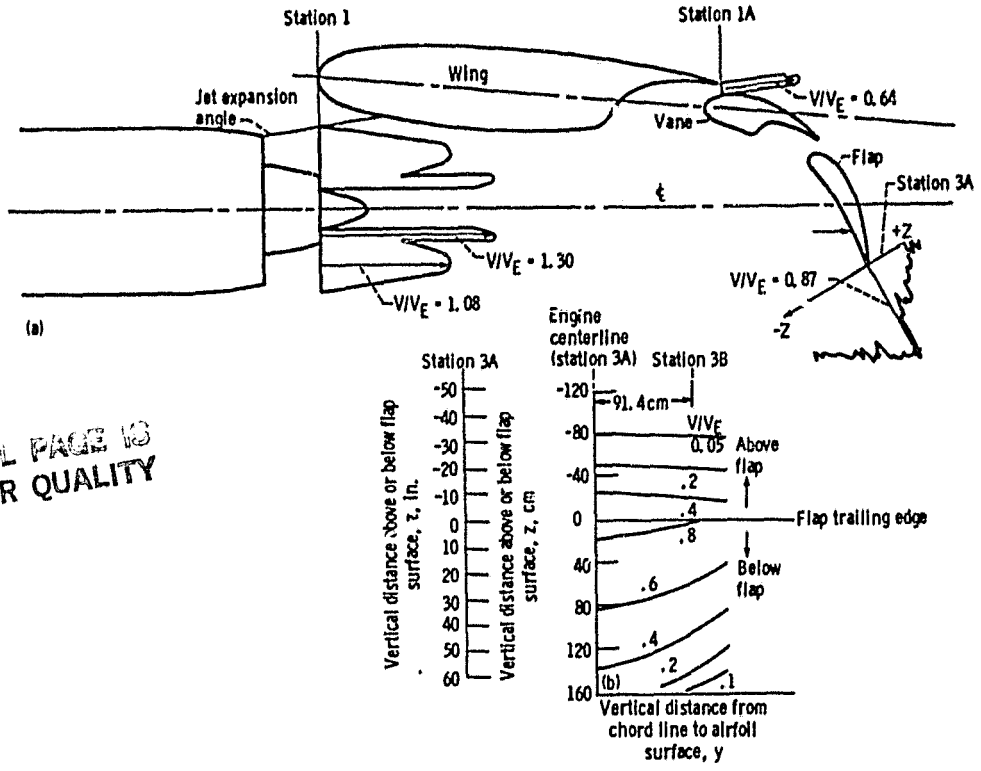


ORIGINAL PAGE IS
OF POOR QUALITY

(a) In plane of engine and span centerlines.
(b) Along span, station 3.

Figure 22. - QCSEE UTW exhaust velocity distribution for approach flap setting at approach power.

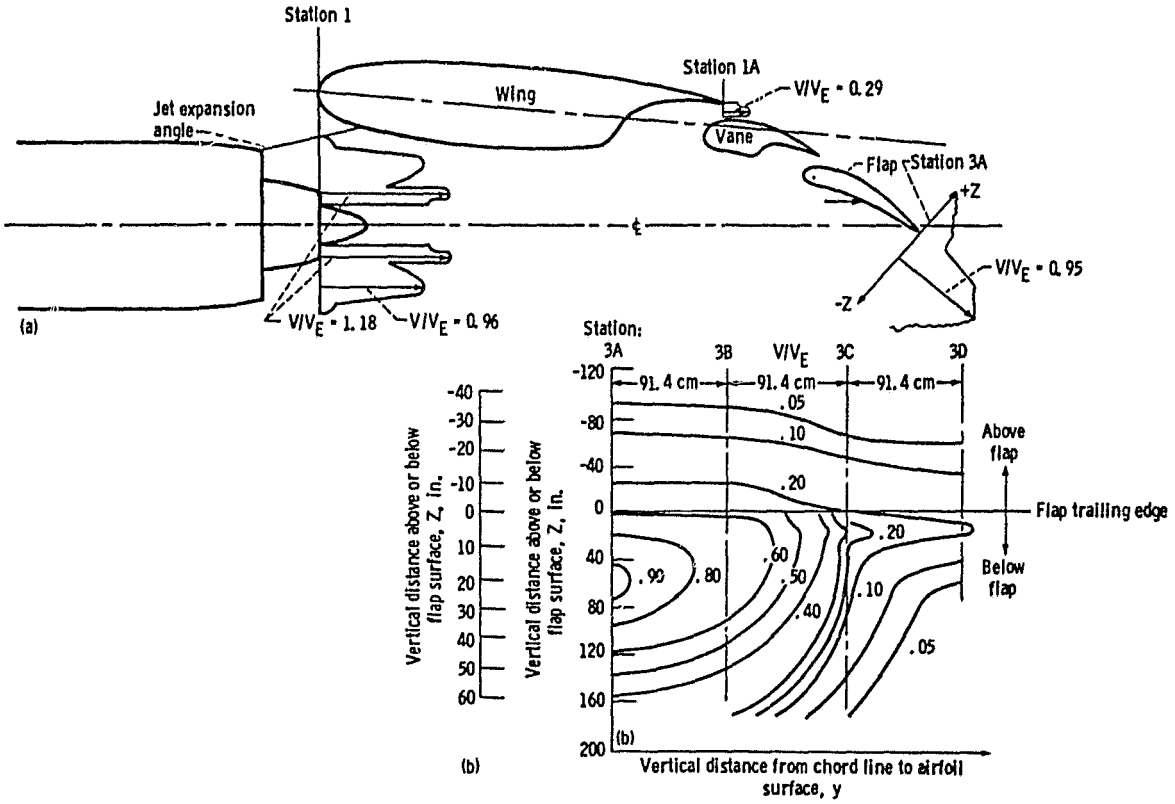


(a) In plane of engine and span centerlines.
(b) Along span, station 3.

Figure 23. - QCSEE UTW exhaust velocity distribution for takeoff flap setting at takeoff power.

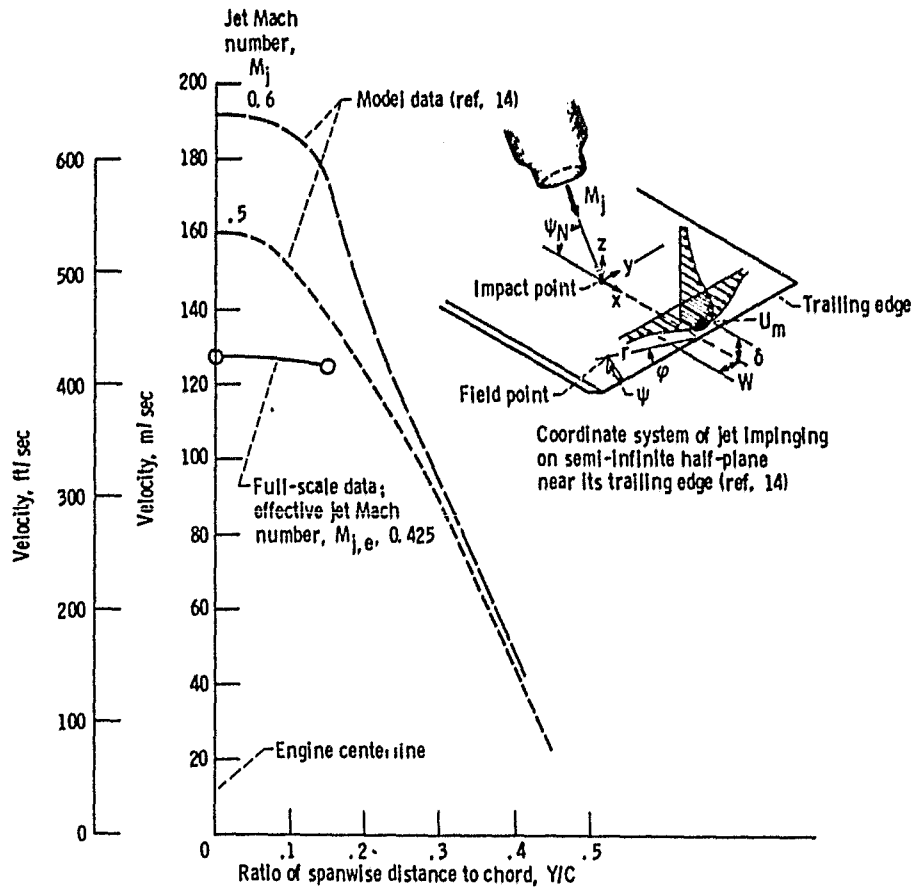


Figure 24. - Comparison of spanwise velocity profile model data from reference 14 with full-scale QCSEE UTW engine test data - approach flap setting at approach power. Ratio of vertical distance from flap to chord, Z/C, 0.03125.

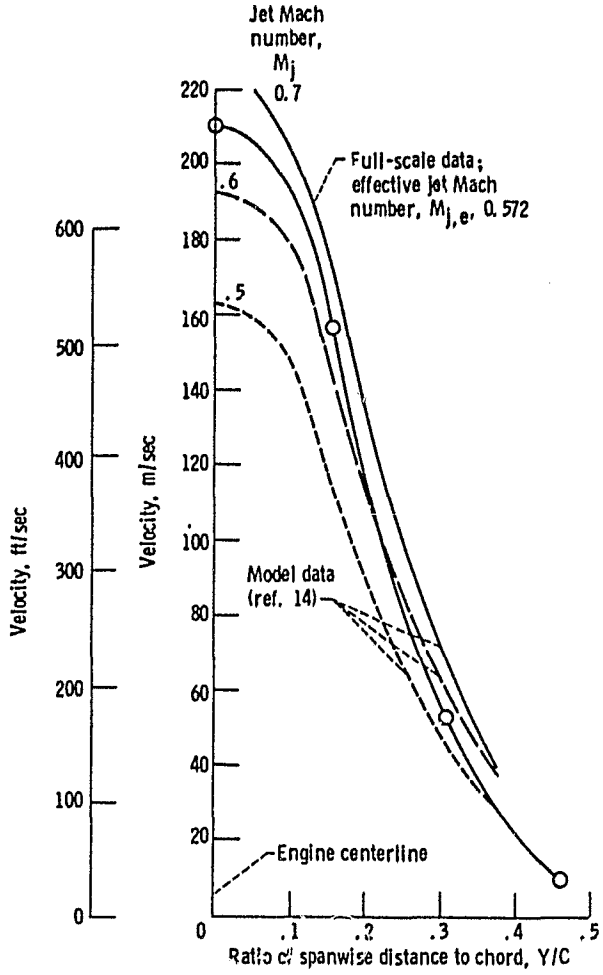


Figure 25. - Comparison of spanwise velocity profile model data from reference 14 with full-scale data - takeoff flap setting at takeoff power. Ratio of vertical distance from flap to chord, Z/C, 0.0834.

ORIGINAL PAGE IS
OF POOR QUALITY

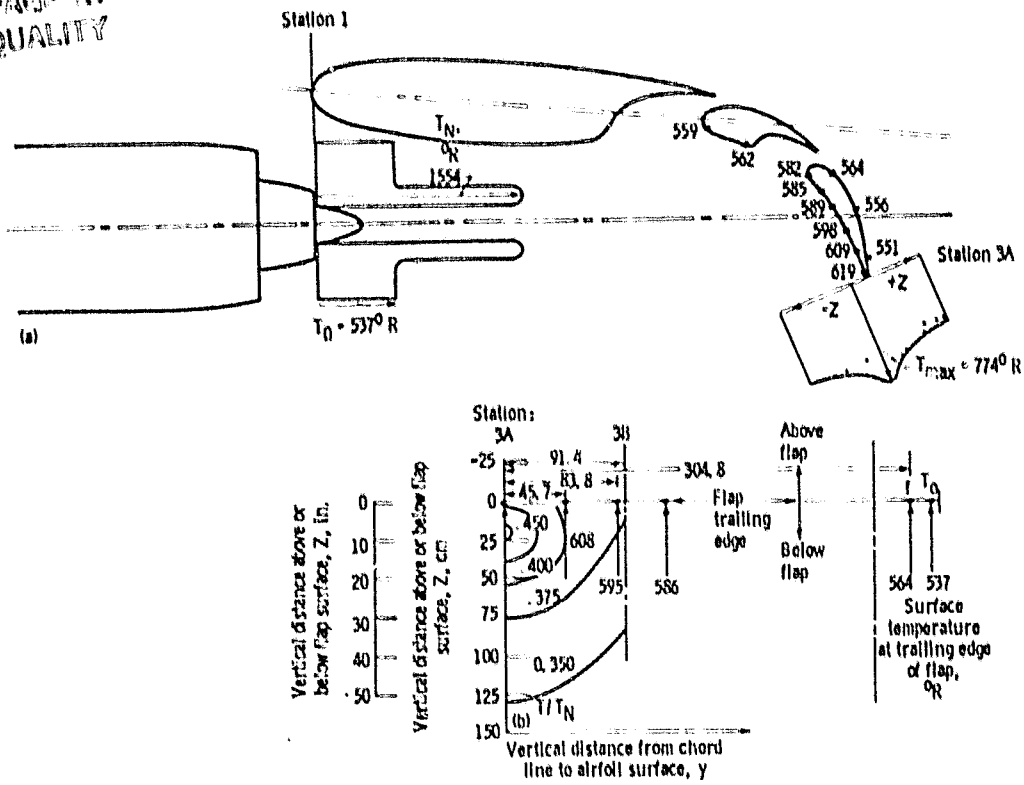


(a) In plane of engine and span centerlines.
(b) Along span, station 3. (Dimensions are in centimeters.)

Figure 26. - QCSEE UTW exhaust temperature and surface temperature distribution for approach flap setting at approach power.

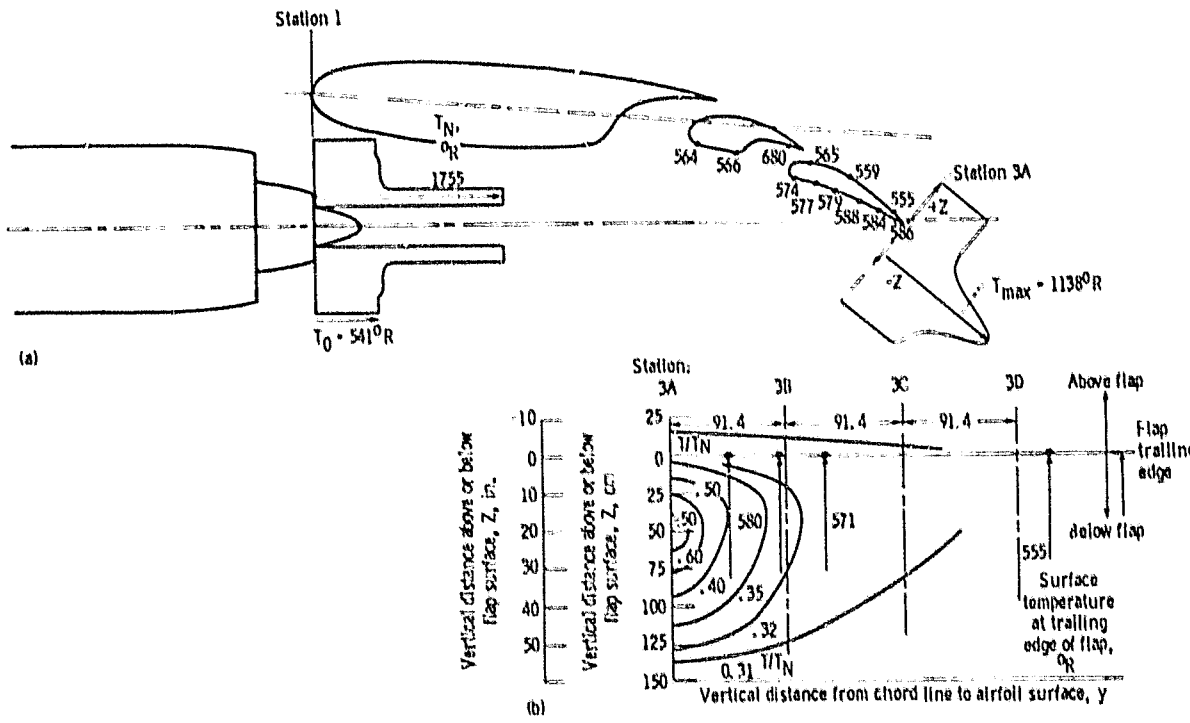


(a) In plane of engine and span centerlines.
(b) Along span station. (Dimensions are in centimeters.)

Figure 27. - QCSEE UTW exhaust temperature and surface temperature distribution for takeoff flap setting at takeoff power.

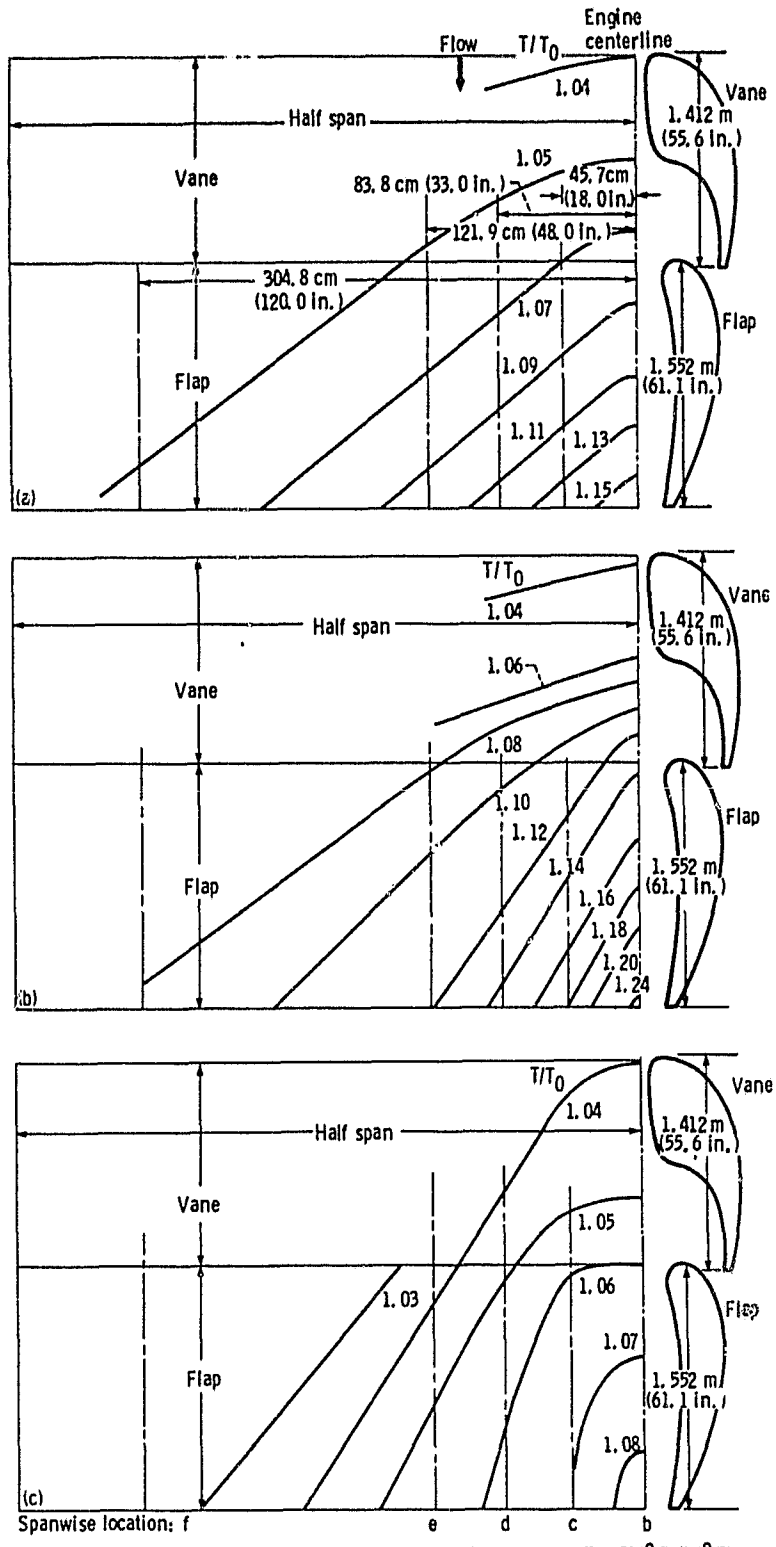


(a) Approach flap setting at approach power. Ambient temperature, $T_0$, 536° R (76° F).

(b) Approach flap setting at takeoff power. Ambient temperature, $T_0$, 539° R (79° F).

(c) Takeoff flap setting at takeoff power. Ambient temperature, $T_0$, 541° R (81° F).

Figure 28. - Bottom-surface temperature contours on vane and flap.

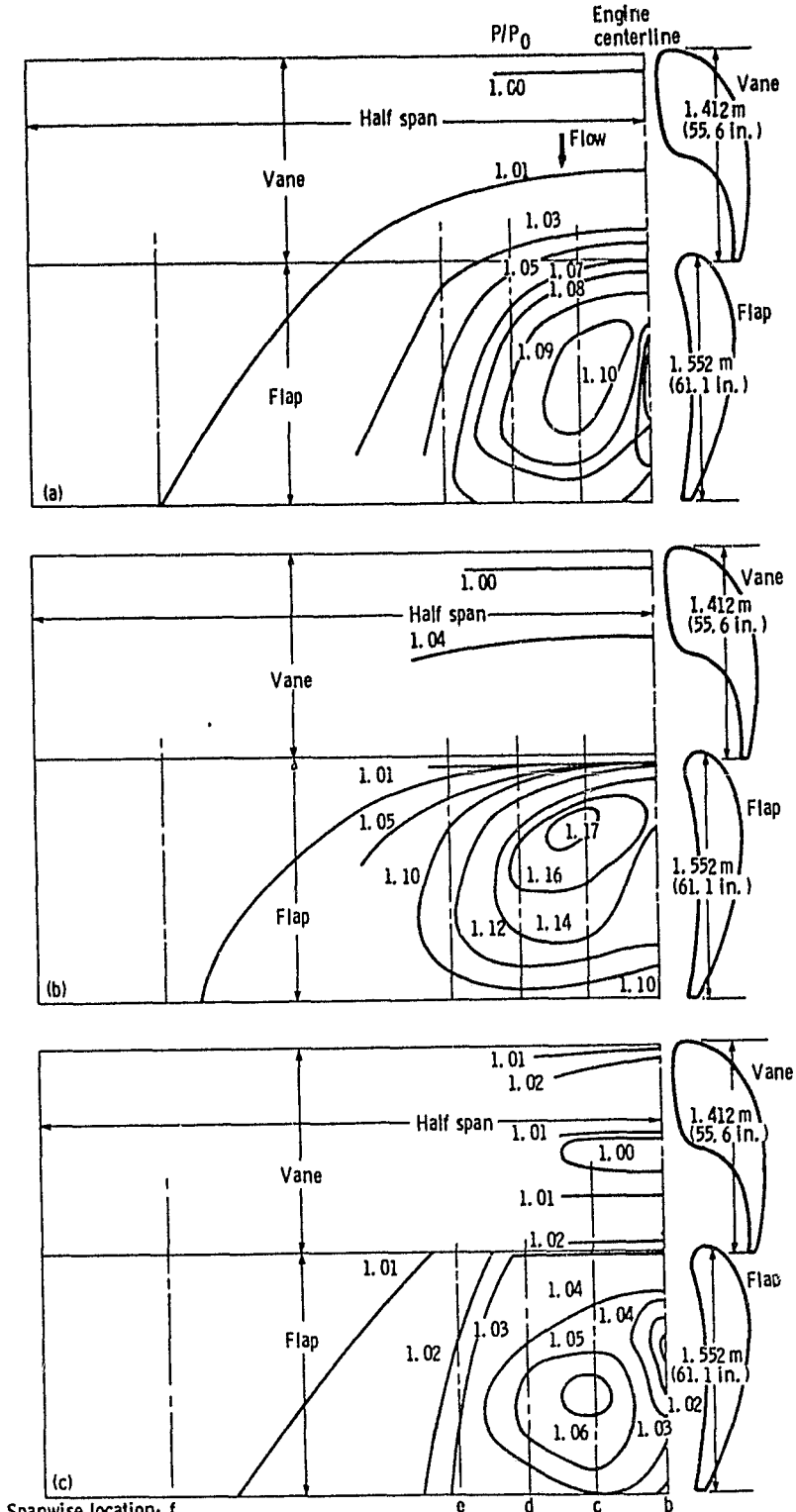


(a) Approach flap setting at approach power. Ambient pressure, $P_0$, $0.986 \times 10^{-5}$ Pa (14.313 psia).

(b) Approach flap setting at takeoff power. Ambient pressure, $P_0$, $0.9864 \times 10^{-5}$ Pa (14.311 psia).

(c) Takeoff flap setting at takeoff power. Ambient pressure, $P_0$, $0.9931 \times 10^{-5}$ Pa (14.407 psia).

Figure 29. - Bottom-surface static pressure contours on vane and flap.

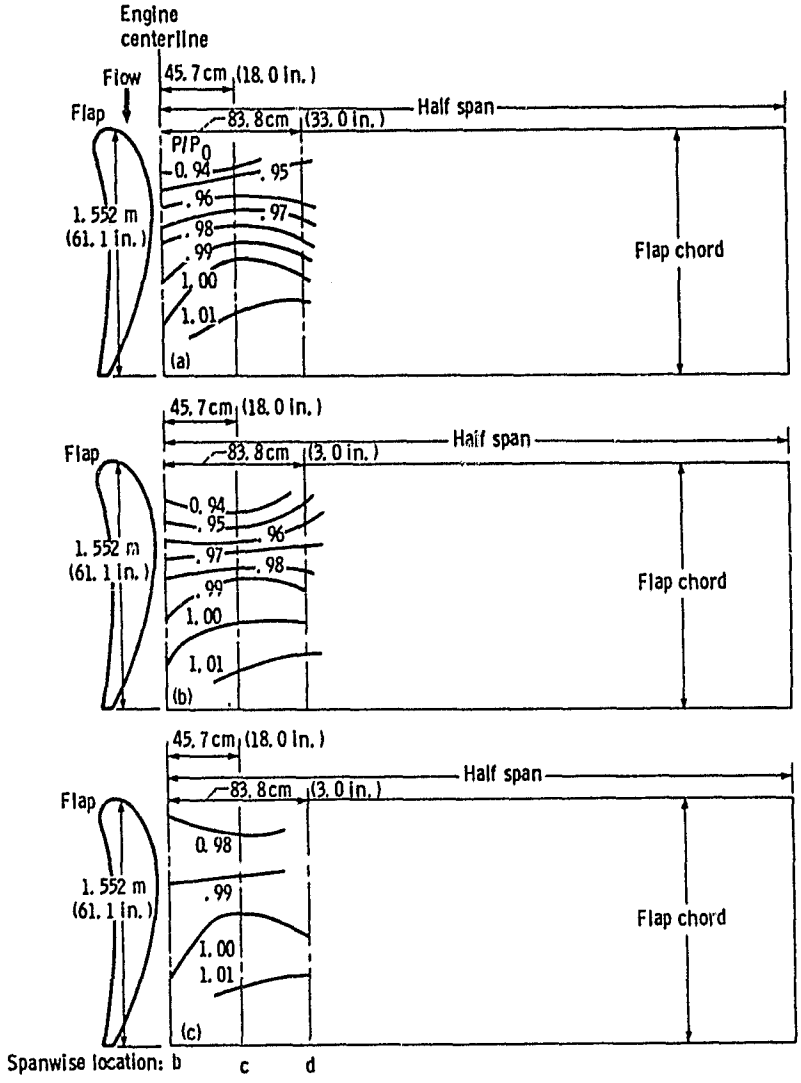


(a) Approach flap setting at approach power. Ambient pressure, $P_0$, $0.9865 \times 10^{-5}$ Pa (14.313 psia).

(b) Approach flap setting at takeoff power. Ambient pressure, $P_0$, $0.9864 \times 10^{-5}$ Pa (14.311 psia).

(c) Takeoff flap setting at takeoff power. Ambient pressure, $P_0$, $0.9931 \times 10^{-5}$ Pa (14.407 psia).

Figure 30. - Top-surface static pressure contours on vane and flap.

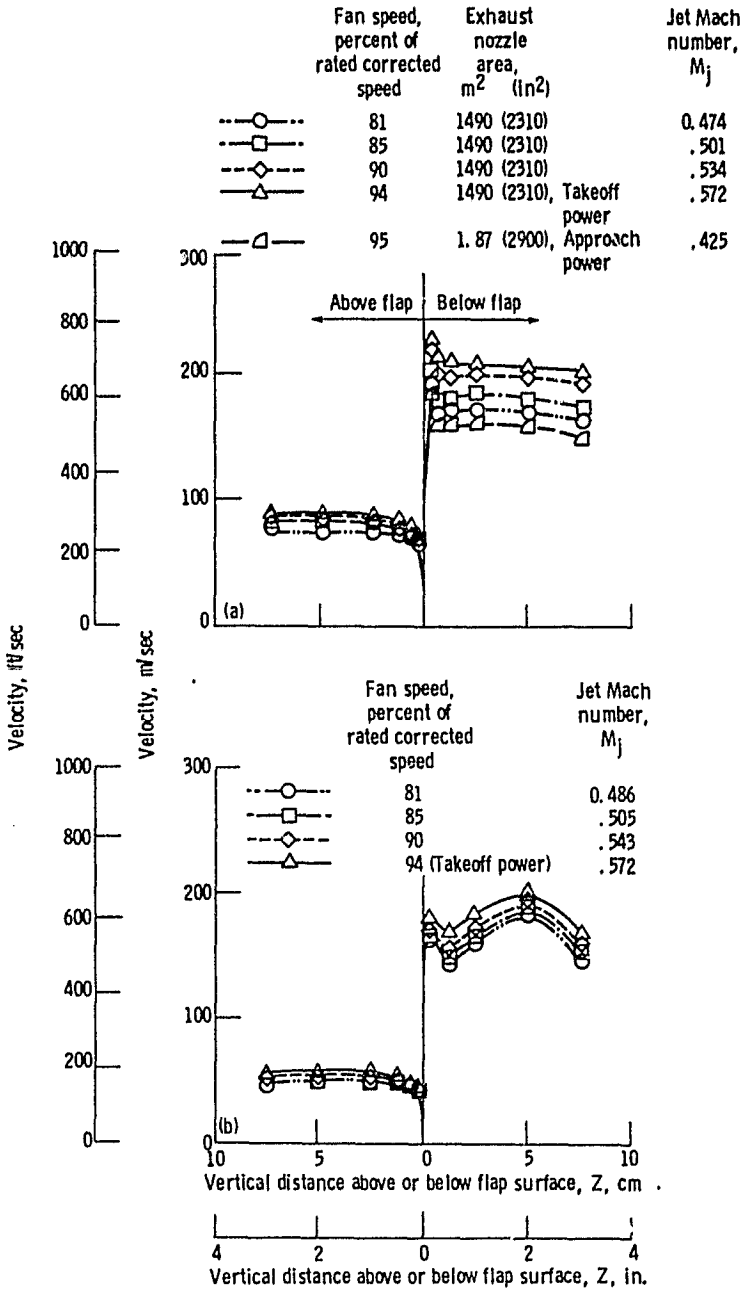


(a) Approach flap setting.

(b) Takeoff flap setting.

Figure 31. - Effect of jet Mach number on boundary layer survey at station 2A.

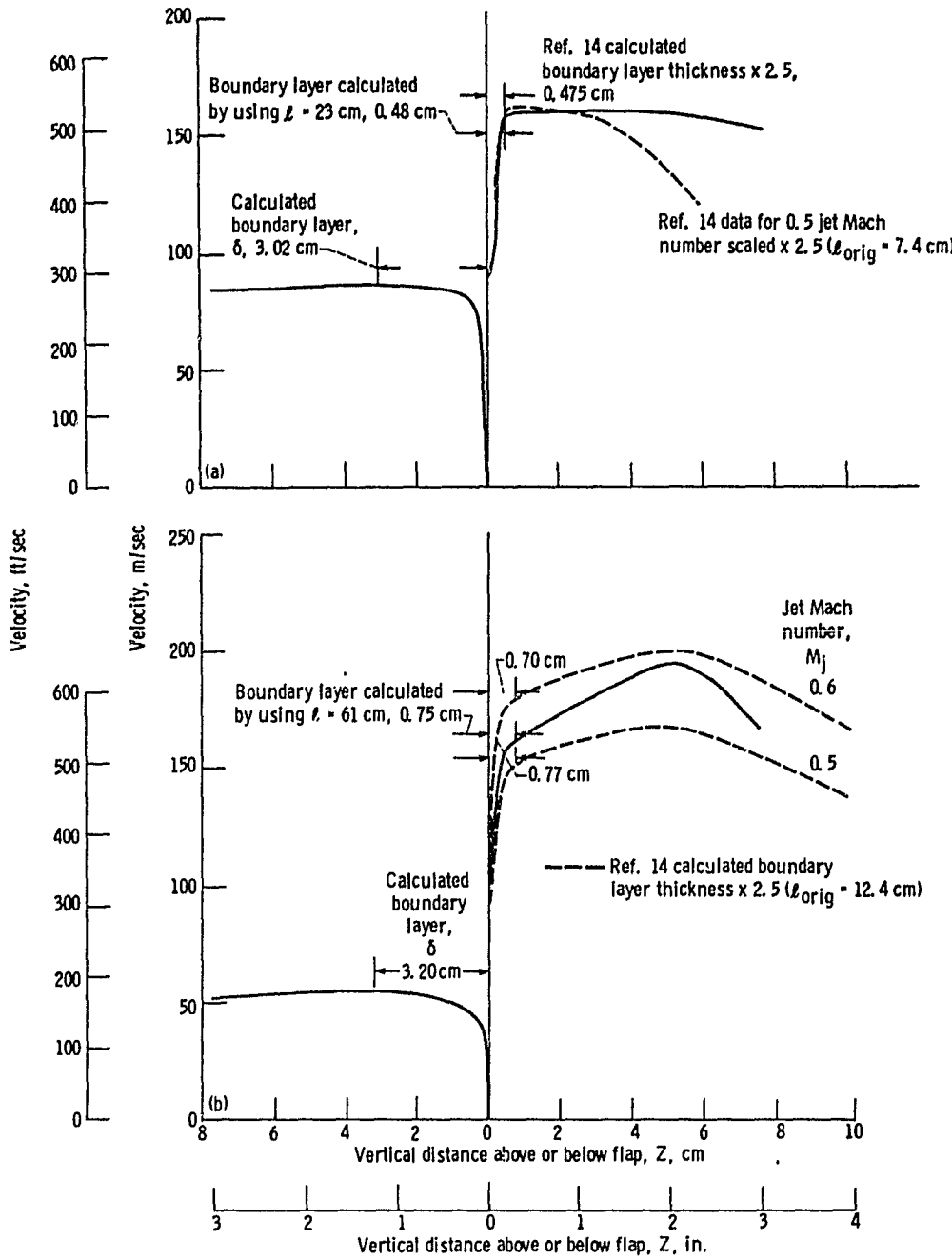


(a) Approach flap setting at approach power. Effective jet exit Mach number, 0.427.

(b) Takeoff flap setting at takeoff power. Effective jet exit Mach number, 0.572.

Figure 32. - Boundary layer profile at station 2A.